
Universidade de Aveiro Departamento de Física
2008

José Carlos Vieira Leitão

Estudo e optimização de materiais para aplicações termo-magnéticas

Universidade de Aveiro Departamento de Física
2008

José Carlos Vieira Leitão

Optimização de materiais para aplicações termo-magnéticas

Dissertação apresentada à Universidade de Aveiro para cumprimento dos requisitos necessários à obtenção do grau de Mestre em Física, realizada sob a orientação científica do Dr. Vítor Amaral, Professor Associado do Departamento de Física da Universidade de Aveiro, e co-orientação do Dr. Mário Reis, Investigador Auxiliar do laboratório Associado CICECO, da Universidade de Aveiro

Dedico este trabalho aos meus santos pais, pela cobertura semi-total de todas as minhas despesas de estudo e sem a qual, logicamente, este trabalho nunca poderia existir.

o júri

presidente

Prof. Dr. Armando José Trindade das Neves
professor associado do Departamento de Física da Universidade de Aveiro

Prof. Drª. Maria Benilde Faria de Oliveira e Costa
professora auxiliar do Departamento de Física da Universidade de Coimbra

Prof. Dr. Vítor Brás Sequeira Amaral
professor associado do Departamento de Física da Universidade de Aveiro

Dr. Mário de Souza Reis Júnior
Investigador auxiliar do CICECO, Universidade de Aveiro

agradecimentos

O autor do corrente trabalho gostaria de agradecer ao grupo magnetocalorico da Universidade de Aveiro, Dr. Vítor Brás de Sequeira Amaral (orientador de Mestrado), Dr. Mário de Souza Reis (co-orientador de Mestrado), Prof. Joaquim Vieira, Dr. Daniel Rocco, Dra. Soma Das, M.Sc João Amaral e M.Sc Rodrigo Pacher Fernandes, tanto pelo apoio técnico-científico como pelo seu companheirismo; também aos M.Sc. A. M. Pereira e Dr. J. P. Araújo do IFIMUP pela sua ajuda na fusão a arco das nossas amostras e ao Mário Seabra, do Dep. de Cerâmica e do Vidro da Universidade de Aveiro, sem o qual o corte e polimento das nossas amostras teria sido muito mais difícil.

palavras-chave

Efeito magnetocalorico, Ni_2MnGa, liga de Heusler, memoria de forma, anisotropia magnetica, $PrNi_{5-x}Co_x$, percolação, reorientação de spin, RNi_2, modelo Hamiltoniano.

resumo

O presente trabalho pretende estudar e optimizar a aplicação de materiais magnéticos para dispositivos termomagnéticos. Assim, estudámos as séries $Ni_2MnGa_{1-x}Bi_x$ (com x de 0 a 0.05), $PrNi_{5-x}Co_x$ (com x entre 1.95 e 3.00) e RNi_2 (com R=Tb;Nd;Gd).

Para a série $Ni_2MnGa_{1-x}Bi_x$ estudámos a influência da substituição de bismuto numa tentativa de aproximar, e possivelmente juntar, as temperaturas de transição estrutural e magnética, T_M e T_C, juntamente com o estudo da anisotropia magnética desta liga. Os nosso resultados de facto mostram a aproximação de T_M e T_C, provocado pelo aumento do parâmetro de rede *a* e do aumento da concentração electrónica das amostras dopadas, embora a dopagem estudada não tenha sido suficiente para juntar as duas temperaturas. Encontrámos um máximo de variação de entropia magnética de 3.8 J/kg.K para a amostra pura e de 2.2 J/kg.K para a amostra com o máximo de dopagem (0.05).

Na serie $PrNi_{5-x}Co_x$, devido á competição entre as energias de anisotropia das sub-redes de Co e Pr esta série apresenta uma reorientação de spin a baixa temperatura (~140K). Esta série apresenta um rico diagrama de fases magnéticas, que foi construído no presente trabalho e alguns efeitos ratificados baseando-se na teoria de percolação. Também encontramos um largo pico de entropia magnética associado ao processo de reorientação de spin e à transição magnética.

No que toca á serie RNi_2 o nosso estudo apenas se limitou a produção, análise da homogeneidade e cálculo de variação de entropia magnética das amostras, para posterior estudo pelo Dr. Pedro J. von Ranke (Universidade Estadual do Rio de Janeiro) utilizando um modelo Hamiltoniano teórico para simular as propriedade magnetocaloricas da serie RNi_2. As amostras $TbNi_2$ e $GdNi_2$ mostraram ser monofásicas embora a de $NdNi_2$ não. O modelo teórico utilizado mostrou ser muito eficiente a prever o comportamento magnético das amostras.

keywords

Magnetocaloric effect, Ni_2MnGa, Heusler alloy, memory shape, magnetic anisotropy, $PrNi_{5-x}Co_x$, percolation, spin reorientation, RNi_2, Hamiltonian model.

abstract

The present work intends to study and optimize the application of magnetic materials for thermal-magnetic devices. As such we have studied the series $Ni_2MnGa_{1-x}Bi_x$ (with x from 0 to 0.05), $PrNi_{5-x}Co_x$ (with x in the interval 1.95 to 3.00) and RNi_2 (com R=Tb;Nd;Gd).

For the $Ni_2MnGa_{1-x}Bi_x$ series we studied the influence of the bismuth substitution in an attempt to o make the magnetic and structural transition temperatures, T_C and T_M, come closer and possible merge, in addition, we also study the magnetic anisotropy of this alloy. Our results have in fact increased T_M and decreased T_C, caused by the increase of the lattice parameter *a* and the increase of the electron concentration of the alloyed samples, although the studied alloying was not enough to merge the two temperatures. We found a maximum magnetic entropy change of 3.8 J/kg.K for the pure sample and 2.2 J/kg.K for the sample with the most alloying (0.05).

In the $PrNi_{5-x}Co_x$ series, due to the competition between the anisotropy energies of both the Co and Pr sub lattices this series has a spin reorientation phenomenon at low temperature (~140 K). This series presents a rich magnetic phase diagram that was constructed in the present work and some effects ratified based on the percolation theory. We also found a large magnetic entropy change peak due to the spin-reorientation process and the magnetic transition.

As far as the RNi_2 series goes, our study was only limited to the production, homogeneity analyses and magnetic entropy variation calculation, for further study by Dr. Pedro J. von Ranke (State University of Rio de Janeiro) using a theoretical Hamiltonian model to simulate the magnetic properties of the RNi_2 series. The $TbNi_2$ and the $GdNi_2$ samples have shown to be single phase while the $NdNi_2$ does not. The theoretical model has shown to be very effective in predicting the magnetic behavior of the samples.

Contents

List of Figures

List of Tables

Chapter 1

Introduction

1.1 Fundamentals of the Magnetocaloric Effect

The magnetocaloric effect (MCE) is the best chance of creating a more efficient refrigeration technique, both in energy efficiency and environmental friendliness. It is, in simple terms, the increase/decress in temperature of a magnetic material due to the application/removal of a magnetic field, as it can be observed in an adiabatic process. It can also be understood in an isothermal process as a heat exchange between the material and a thermal reservoir, also due to a magnetic field change. From the quantitative point of view, the MCE is measured trough the isothermal magnetic entropy change (ΔS) or adiabatic temperature change (ΔT_{ad}), Figure (1.1); both quantities derived from thermodynamic relationships and, to obtain those, the measurements of magnetization and specific heat as a function of temperature and magnetic field are needed.

It is straightforward the idea of producing a thermo-magnetic cycle based on the isothermal and/or adiabatic processes, using therefore the Brayton (adiabatic) and Ericsson (isothermal) cycles, respectively; and indeed this idea begun in the late 1920s, when cooling via adiabatic demagnetization was proposed by Debye [1] and Giauque [2]. The process was latter demonstrated by Giauque and MacDougall in 1933, by which they reached 250 mK [3]. Since then, the adiabatic demagnetization has been used within some specific contexts; namely, to cool NASA-XRS detectors (1.5 K).

On the other hand, room temperature magnetic cooling device technology, having been actively studied since 1976, as a result of a seminar paper by Brown [4], witch showed that a continuously operating device working near room temperature could achieve much larger temperature spans than the maximum observed magnetocaloric effect [4], but even after such a long span of time this technology is sill in an early phase of development, with no commercially available products and only few prototypes. In

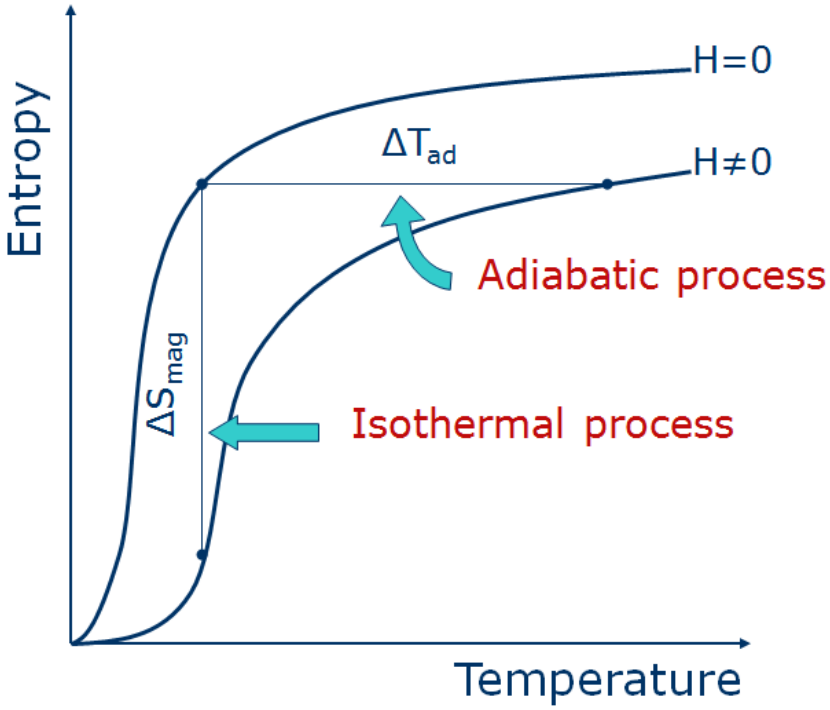

Figure 1.1: Isothermal and Adiabatic Processes

August 2001, Astronautics Corporation of America, USA, announced a prototype of a room temperature magnetic cooler [4]. This prototype has a cooling power of 95 W, and uses as the active magnetic material Gd spheres [5]. Later, in March 2003, Chubu Electric and Toshiba, Japan, also announced the creation of a room temperature magnetic cooler prototype. This machine has a cooling power of 60 W, and uses a layered bed of a Gd-Dy alloy as the active magnetic material [5]. Both of them used permanent magnets of Nd-Fe-B to produce the magnetic field.

In this sense, most of the MCE research developed world wide is devoted to explore and optimize the magnetocaloric properties of known materials, as well as to seek for new magnetocaloric characteristics in new materials, these must have low cost, non-toxicity, good thermal conductivity and a huge and broad ΔS variation vs. temperature.

In this particular work, however, we will only consider the isothermal process and the ΔS to characterize the MCE, using therefore one of Maxwell's relations [6]:

$$\left(\frac{\partial S_M(T,M)}{\partial H}\right)_T = \left(\frac{\partial M(T,H)}{\partial T}\right)_H \tag{1.1}$$

that, in order of the entropy change from a field H_i to H_f , is displayed as such:

$$\Delta S(T)_{\Delta H} = \int_{H_i}^{H_f} \left(\frac{\partial M(T,H)}{\partial T} \right)_H dH \tag{1.2}$$

So, as ΔS is given as the derivative of the magnetization versus temperature, mathematically speaking, as a function of the area between magnetic isotherms, it will be maximum around large changes of magnetization, like the ones that occur near the magnetic transition temperature from the ferromagnetic to the paramagnetic phases (Curie Temperature T_C), for example.

1.2 Magnetic materials used in magnetic refrigeration

1.2.1 Family R-G (R: rare-earths, G: metalloid)

Since the discovery of the giant MCE in $Gd_5Si_2Ge_2$ (35 J/kgK at 280 K), in 1997 [7], extensive study has been done on this alloy. That large ΔS value (in modulus, ΔS is actually a negative) is due to a coupled magneto-structural first-order transition, driven by temperature [8], magnetic field [9] and pressure [10]. Several series have been studied from this parent compound, namely: (*i*) $Gd_5(Si_{1-x}Ge_x)_4$ alloys, with ΔS ranging from 61 J/kgK at 90 K to 8.6 J/kgK at 340 K [5]; (*ii*) $(Gd,Pr/Tb)_5Si_4$ [11], without any significant change on the magnetocaloric properties; (*iii*) $R_5(Si_{1-x}Ge_x)_4$ alloys, where R means a rare-earth, like Nd [12], Tb [13], Dy [14] and Ho [15]; and (*iv*) many others [5]. Also interest is the work of Morellon et al [10] that could merge the structural and magnetic transition of $Tb_5Si_2Ge_2$ compounds by applying 8.6 kbar of hydrostatic pressure; increasing therefore the MCE.

1.2.2 Family R-M-G (M: transition metal)

Another series with magneto-structural coupling is the $La(Fe_xSi_{1-x})_{13}$ [16]. For instance, ΔS for x=0.88 reaches 26 J/kgK at 188 K. These compounds under a negative pressure (expansion of the unit cell), via insertion of Hydrogen, could shift the transition temperature up to RT [17]; on the other hand, positive pressure (compression of the unit cell), via hydrostatic pressure, increases the ΔS value, decreasing, however, the transition temperature [18]. Substitution of 50% of Pr for La has also been done [19], increasing the value of ΔS for 30 J/kgK at 185 K.

1.2.3 Family Mn-M-G

MnAs is a compound that presents a coupled magneto-structural first order transition, resulting therefore in a huge ΔS: 32 J/kgK at 318 K [20]. Wada et al. [20], studied Mn(As,Sb) and found that both, transition temperature and ΔS decrease by adding Sb; disregarding therefore this series comparing to the parent compound. More recently, Gama et al. [21] applied 2.2 kbar in MnAs compound and could increase the ΔS up to 267 J/kgK at 280 K. Other compounds with Mn are those of the series MnFe(P,As). Tegus et al. [22] pointed out the highest ΔS value of that series: 32 J/kgK at 220 K for the compound $MnFeP_{0.65}As_{0.35}$.

Concerning the Heusler alloys Ni_2MnGa, this material has a decoupled magneto-structural transition of about 100 K. Hu et al. [23] was the first to report the magnetocaloric properties of this compound, and, more recently, Zhou et al. [24] reported a coupled magneto-structural transition for the out of stoichiometry $Ni_{55}Mn_{19}Ga_{26}$, with a huge, but narrow, ΔS: 20 J/kgK at 317 K.

1.2.4 Manganites family ($RMnO_3$)

The MCE of mixed-valency manganites was first measured by Morelli et al. in 1996, for thick films of $La_{2/3}(Ca/Sr/Ba)_{1/3}MnO_3$ [25]. The magneto-structural coupling [26] and the numerous possibilities of exchanging elements in synthesis make manganites a rich field in MCE study.

The substitution of La by other rare-earth ion in $La_{2/3}Ca_{1/3}MnO_3$ or $La_{2/3}Sr_{1/3}MnO_3$ manganite can tune the transition temperature and enhance magnetocaloric properties [27]. Some manganites systems show also a magneto-structural coupling, due to charge/orbital ordering [5, 28]. For instance, Chen and co-workers found a ΔS value of 7.1 J/kg.K near the charge/orbital ordering temperature (161 K) of the $Pr_{0.5}Sr_{0.5}MnO_3$ manganite [29].

1.2.5 Intermetallics family R-M

There are several sub-families, namely the Laves Phase compounds, as RCo_2 [30], RAl_2 [31] and RNi_2 [32], but all of these are not suitable for applications around room temperature due to their low values of ΔS and T_C. On the contrary, those systems are the reason of several theoretical models, due to its interesting, from the academic point of view, magnetocaloric properties [32]. Other compounds can also be cited: Nd_2Fe_{17} (5.9 J/kgK at 325 K) [33], Gd_7Pd_3 (6.5 J/kgK at 323 K) [34], Gd_4Bi_3 (2.7 J/kgK at 332 K) [35] and Gd_2In (4.5 J/kgK at 194 K) [36].

All of those values of ΔS above reported are related to 5 T of magnetic field change.

All of those families above described, and their corresponding compounds, have problems that avoid their immediate application in a magnetic cooling device. We can mention those systems with (i)first order magnetic transition and a consequent thermal hysteresis, producing therefore energy losses during the thermo-magnetic cycle; (ii) high pure rare-earth metals, making them economically unviable; (iii) elements that need special handling, for instance the poisonous Arsenic; (iv) narrow ΔS curve, avoiding therefore a wide thermo-magnetic cycle and, finally, (v) low values of ΔS, decreasing the cooling power of the device.

1.3 Magneto-structural coupling

As referred above, for MCE application purposes, most magnetic materials are studied regarding their magnetic transition from the paramagnetic to the ferromagnetic, ferrimagnetic, or antiferromagnetic phases [37]. But many of these, besides this 2^{nd} order magnetic transition, undergo a structural 1^{st} order/discontinuous transition, which also involves an entropy changes [38].

In typical systems the dominant entropy change is associated with the 1^{st} order phase transition [38], but in some systems it is possible to merge the two transitions, or at least bring them into close proximity, creating a coupled transition with interesting results for the entropy change. This is due to the coincidence of a 1^{st} order magnetic transition and its attendant structural phase change with a 2^{nd} order magnetic transition [38].

In this case, both the magnetic and crystallographic sub lattices are easily affected by the magnetic field when it is applied [37]. The MCE of materials undergoing coupled magneto-structural transformations arises from the added difference of the entropies of the two crystallographic modifications (polymorphs) of the material [37], creating what is usually called the Giant Magnetocaloric Effect (GMCE).

The phenomenon of coupled magnetic and structural phase transitions is very rare in condensed-matter physics [39] and is usually achieved by careful compositional tuning.

Alloys where such an effect is achievable are, for example, the Gd-Si-Ge alloys [37] and the Ni-Mn-Ga alloys [40] (discussed in the present report).

Chapter 2

$Ni_2MnGa_{1-x}Bi_x$ memory shape alloys

The Ni_2MnGa Heusler alloy is widely studied due to its particular magnetic properties and applications. We can cite, for instance, the memory shape properties and a first order structural transition from martensitic to austenitic phase [22, 41], both of which are ferromagnetic. Free-standing Ni-Mn-Ga thin films have also been used into the first prototypes of microactuators, for optical applications [42]. The studied Ni_2MnGa alloy has a critical temperature T_C of about 375 K [41, 43–46], and undergoes a structural transition between tetragonal martensitic and cubic austenitic phase at a temperature T_M at about 200 K [22, 41, 43, 44, 46]. It has a saturation magnetization, M_S, of 4.17 μ_B/FU[1] below the structural transition temperature T_M [43, 46, 47] and 3.90 μ_B/FU above [46]. Accompanying both the magnetic transition at T_C and the structural transition at T_M this alloy presents large magnetocaloric effect (MCE), with a considerable magnetic entropy change.

The structural transition at T_M has an entropy change of 5 J/kg.K [46], while the magnetic transition at T_C has -1.29 J/kg.K [47], both with a magnetic field change of 1 T. However, this alloy has a high compositional sensitivity, and both transitions have been coupled into a single one, either by, changing the stoichiometry by the partial substitution of Ni for Mn [38, 39, 48] as $Ni_{2+x}Mn_{1-x}Ga$, which results in the merging of the two transitional temperatures at a composition range of 0,18≤ x≤ 0,20 [40, 41, 49], or, by substituting some elements into the alloy ,Cu for instance, in the composition $Ni_2Mn_{0.75}Cu_{0.25}Ga$, having achieved T_C=T_M=308 K (room temperature) [44,50]. These joint transitions have a magnetic entropy change of about 20 J/kg.K with a magnetic field variation of 1 T [49]. This, as referred above, was called the giant magnetocaloric effect (GMCE).

An interesting study by Söderberg *et al* [51] has shown the results of a fourth element addition in the Ni_2MnGa alloy. Although the objective of the referred paper

[1] FU=formula units

was only to study the variation of the transition temperatures, among the various elements added to the alloy an addition of 2% Bi has shown to also increases T_M and decrees T_C.

As such, we aim to study a series of Ni_2MnGa_{1-x},Bi_x alloys, to verify if T_M and T_C merge is possible, and if so, in a usable temperature for magnetic refrigeration at room temperature. Also, we aim to study the high magnetic anisotropy of the two phases (martensitic and austenitic) of pure and Bi substituted alloys through measurements of the magnetization and magnetic entropy change to see what influence and limitation this may have on the possibility of using this alloy in practical magnetic cooling devices.

2.1 Experimental Procedure and Characterization

2.1.1 Sample Preparation

We have prepared four samples: one pure Ni_2MnGa sample, without Bismuth, (sample 1) and three other samples with Bismuth, with x=0.005 (sample 2), x=0.02 (sample 3) and x=0.05 (sample 4). All of the samples were prepared in a Buhler arc melting furnace, at IFIMUP-University of Porto, with the appropriate amount of constituent elements. The furnace works with a water-cooled copper crucible and was pre-evacuated better than $2x10^{-6}$ mbar and refilled with high-purity argon gas. The samples were arc melted twice to obtain homogeneous samples. Afterwards the samples were subjected to heat treatment. The samples were sealed in evacuated quartz tubes and annealed at 1260 K for 10 days and then quenched in water. From our previous experience [46] we decided to, as a secondary treatment, manually grind the samples in an agate mortar and pestle, compact them with a force of 5 tones ($\approx 5x10^8$ N/m^2) and sinterize them wrapped in Tantalum and encapsulated in vacuumed quartz tubes for 10 more days at 1260 K.

The author of this report did not participate in the steps above described.

2.1.2 Crystallography and structural characterization

1º - X-ray diffraction

This analysis was performed at the University de Trás-os-Montes e Alto Douro (UTAD) using a multichannel x-ray diffractometer with a Cu and Kα radiation. Then, using the refinement procedure with the PowderCell software, the crystal structure and lattice parameters were analyzed and revealed them to be single phased, at least within the X-ray resolution, i.e., possible impurity phase is lower than 5% vol.

X-ray diffraction performed on the Bismuth alloyed samples before the second treatment revealed a small quantity of segregated Bismuth, indicating that the Bismuth was not fully incorporated in the microstructure of the material, a result similar to our previous work [46]. However x-ray diffractions after the grinding, compacting and sinterizing no longer show this segregation, meaning that the Bismuth has completely entered the lattice, as shown in Figure (2.1).

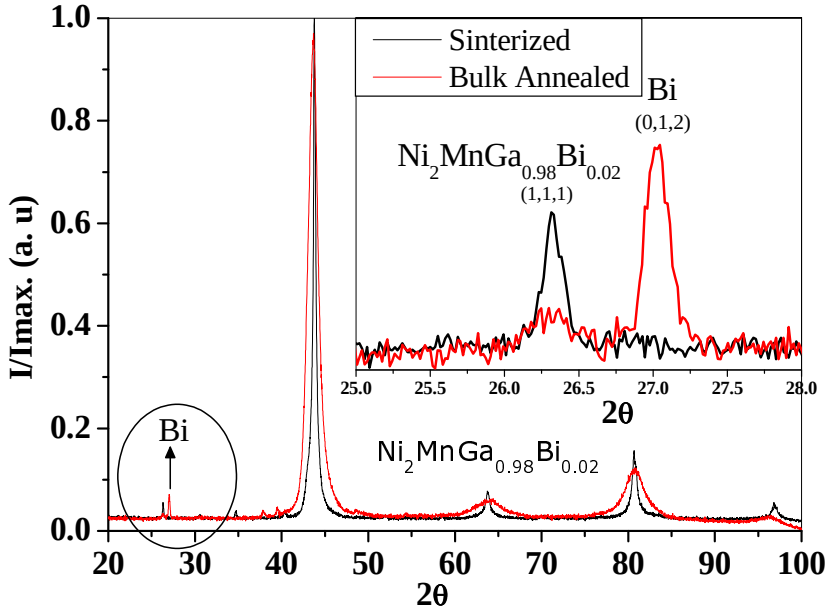

Figure 2.1: X-ray of sample 3 revealing the segregated bismuth before sinterization and a pure phase after. Detail in the inset.

Using Rietveld refinements we measured a lattice parameter of 5.8166 Å, similar in all samples, possibly due to the small percentages of Bismuth used. This system crystallizes in a cubic structure with Fm3m space group, for the austenitic phase (room temperature).

2º - Energy dispersive x-ray spectroscopy (EDS)

In order to check the homogeneity and stoichiometry of the samples, an EDS/SEM (Scanning electron microscope) was used, more precisely the Phillips-FEI/Quanta 400, from UTAD. To achieve a more reliable result, up to six measurements were performed on each sample. These results can be obtained within 5% of certainty.

The EDS technique indicates deviations that are less than 5% when compared with the nominal atomic percentage for each sample. It is still important to note that the composition variation of the analysis is sometimes within this value.

EDS measurements confirmed the previously stated. No segregation or secondary phases are observed in the sinterized samples. Small white balls are visible but careful

zoom reveals that their composition is the same as the rest of the sample. This can be observed in our SEM photos in Figure (2.2).

2.1.3 Magnetic measurements

The magnetic measurements M(T,H) were performed with a vibrating sample magnetometer (VSM) at the University of Aveiro, with a field range from 0 to 10 T and a temperature range from 5 to 300 K. At IFIMUP-University of Porto, also using a VSM magnetometer we had access to a temperature range from 300 to 500 K, with a field range of 0 up to 1 T.

2.2 Magnetic properties

In order to check the variations of T_M and T_C of our bismuth alloyed samples we measured magnetization in order o temperature for small fields. The results can be seen in Figure (2.3).

There was a decrease in the thermal hysteresis around T_C for the alloyed samples. Hysteresis has dropped from 6 K for sample 1 (without Bi) to under 1 K in all the other samples. This is an important point when studying material for the creation of a practical magnetic refrigerator, a big hysteresis will mean that the thermal-magnetic cycle of the refrigerator will have losses and won't be sufficiently efficient, also, in transitions with a large hysteresis the Maxwell relation used to calculate the MCE (Eq. (1.2)) loses its viability, giving rise to super estimated values of ΔS. On the other hand, the hysteresis of the structural transition has increased, from 11 K for the sample 1 to 20 K in all other samples. T_M has changed from 200 K to 219 K and T_C from 375 K, in the pure sample, to 368 K in all alloyed samples. Taking into account these results we can only conclude that this change was completely due to the bismuth alloying. This only comes to highlight how bismuth alloying is efficient at producing this effect. These changes were equal in all alloyed samples and can be viewed in Figure (2.4).

As far as the structural transition goes, the composition changes of Ni-Mn-Ga alloys change the electron concentration (e/a) and this parameter is usually thought to be the way the composition influences T_M in the Ni-Mn-Ga alloys [52].

The e/a can be roughly defined as the range of the average number of valence electrons per atom [53]. Knowing that in a pure Ni_2MnGa alloy e/a is about 7.50 (adimensional) [54] and Söderberg's bismuth alloyed sample, in the stoichiometry $Ni_{2.008}Mn_{1.096}Ga_{0.844}Bi_{0.052}$, had an e/a of 7.636 [51], we can easily assume that all

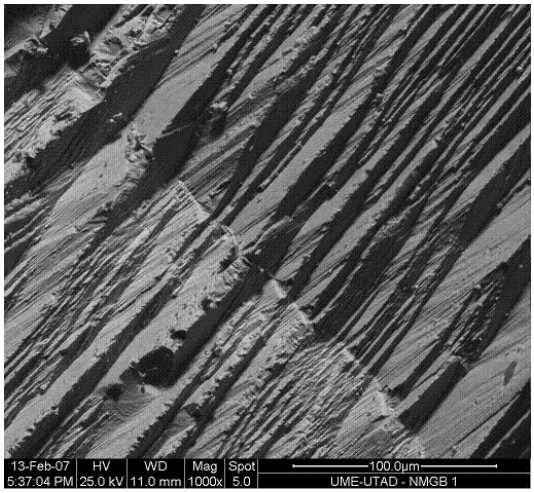

(a) SEM photos of Ni_2MnGa (x1000 magnification), not sinterized

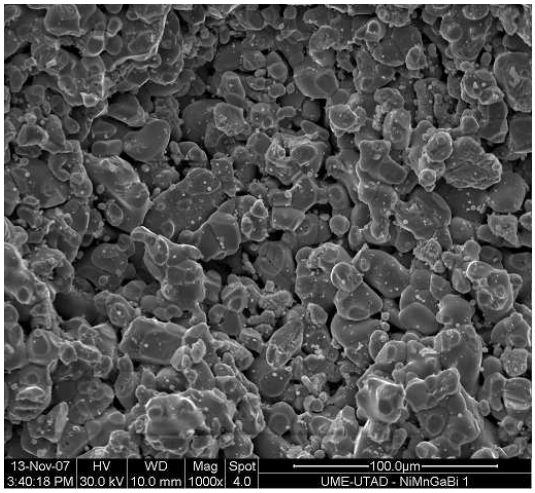

(b) SEM photos of $Ni_2MnGa_{0.995}Bi_{0.005}$ (x1000 magnification)

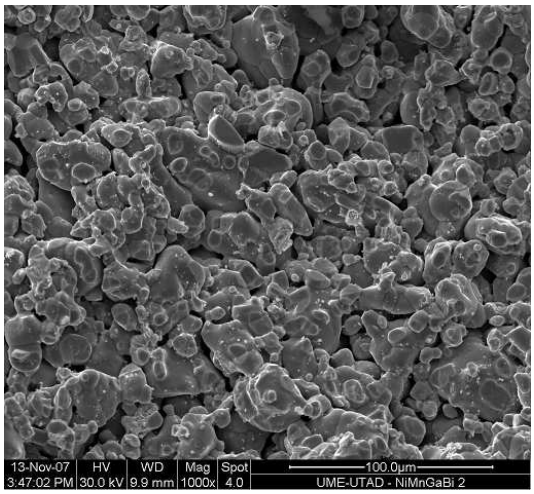

(c) SEM photos of $Ni_2MnGa_{0.98}Bi_{0.02}$ (x1000 magnification)

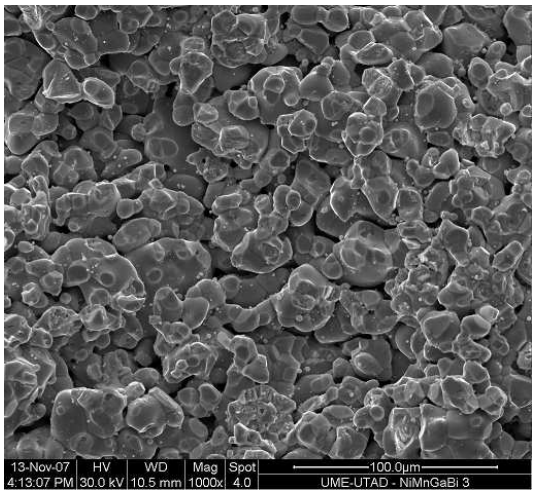

(d) SEM photos of $Ni_2MnGa_{0.95}Bi_{0.05}$ (x1000 magnification)

Figure 2.2: SEM photos of all the $Ni_2MnGa_{1-x}Bi_x$ samples

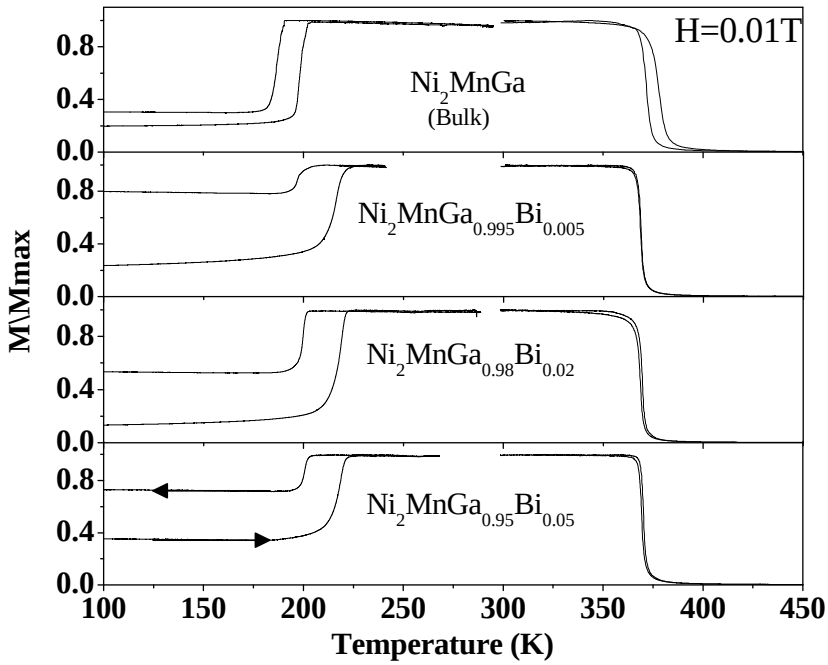

Figure 2.3: Magnetization as a function of temperature, for all samples prepared, i.e., from 0% up to 5% of Bi in the Ga site. We can observe an increasing of T_M transition and decreasing of T_C, by adding Bi.

our alloyed samples (sample 2, 3 and 4) had a bigger e/a than our pure sample (sample 1). If we are removing Ga atoms ([Ar] $3d^{10}$ $4s^2$ $4p^1$) and replace them with Bi atoms ([Xe] $4f^{14}$ $5d^{10}$ $6s^2$ $6p^3$), then, logically we will be increasing the number of valence electrons in the unit cell. As such, Chen *et al* [52] show that T_M increases with e/a.

In terms of band model, the effect of e/a on T_M can be explained as follows. The $L2_1$ crystal structure was stabilized because the Fermi surface just touches the (110) Brillouin zone, in this way periodic structure of the crystal exists [52]. When the electronic concentration in the crystal structure increases, the Fermi surface and the (110) Brillouin zone overlap, electrons above the Fermi level move to the corner states of the Brillouin zone, and the excessive increasing of energy of system results in the distortion of the lattice to minimize the free energy, which leads to the formation of the martensite [52, 55].

Chen [52] also tells us that based on electronic theory of metals [56], the radius of the Fermi sphere, k_F, is a function of the density of valence electrons, n, only. The decrease of n will result in the decrease of k_F thereby the energy of system, which leads to a stable state. According to the above, the density of valence electrons can be used to analyze the way composition affects martensitic transformation temperature. The density of valence electrons n can be described as:

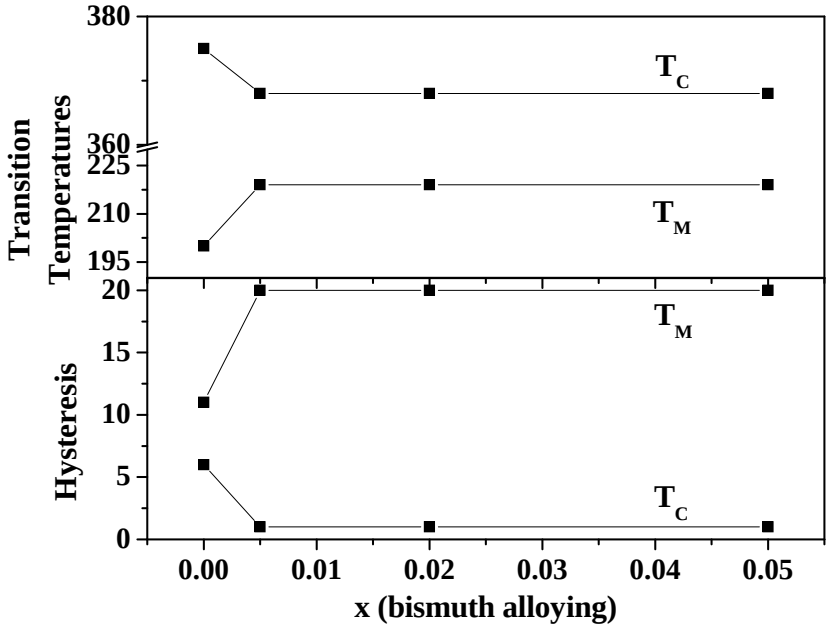

Figure 2.4: Transition temperatures and hysteresis changes in order of bismuth quantity

$$n = \frac{(e/a) \times n_1}{V_{cell}} \tag{2.1}$$

where V_{cell} is the volume of unit cell and n_1 the average number of atoms contained within a unit cell. Seeing as the cell volume of our samples was less than 1% different from each other, we can consider it to be constant, and as the e/a theoretically increases with increasing bismuth we can assume in our alloyed samples that n is increasing. Chen shows us that T_M increases with n [52], once again confirming our results.

Furthermore, Chernenko [57], while studying the compositional sensitivity of Ni-Mn-Ga alloy, concluded that, at constant Mn, T_M is inversely proportional to the Ga content of the alloy, which is also coherent with our results.

Concerning T_C, Söderberg, having observed the same results, attributes the decrease of T_C to the increase of the lattice parameter a, which leads to longer Mn−Mn distance in the structure and a consequent reduction in the exchange interaction between Mn atoms. This should also be our case, as Bi atoms substitute the Ga atoms in the lattice and the distance between Mn atoms increases (see Figure (2.5)).

In fact we did not observe any significant change in the lattice parameter a, but we must take into consideration the small quantities of bismuth used and that our lattice analyzing tools give us only an average of these values. This meaning that in our samples there will be many long stretches of material without a single bismuth atom and we are unable to pinpoint and measure the places were the bismuth has actually entered the lattice.

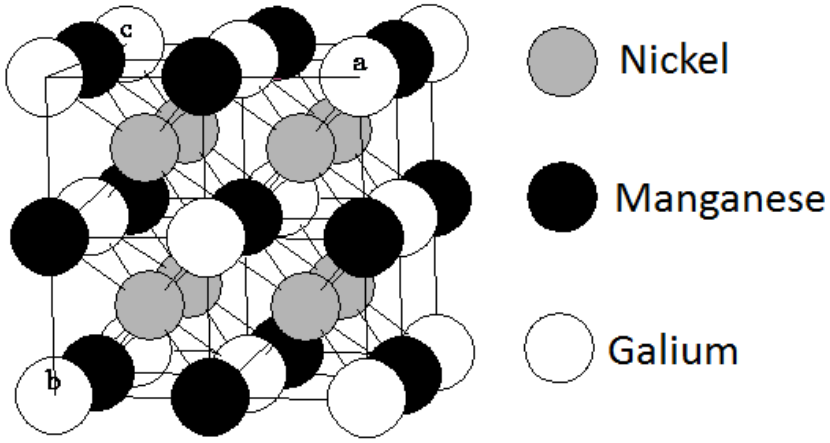

Figure 2.5: Ni_2MnGa unit cell, revealing the Bi and Ga sites, increasing therefore the distance between Mn atoms.

Also, Chernenko [55] related the e/a with both T_M and T_C, reporting the behavior described above concerning T_M, but also showing that, for values of e/a above 7.5 (the ones we are interested in) T_C decreases.

2.3 Influence of the magnetic anisotropy on the magnetic entropy change

From a set of isothermal measurements around T_M, we could obtain the results presented in Figure (2.6), and, using an appropriate Matlab routine created by Dr. Mário Reis, from these we determine the variation of magnetization with temperature, Figure (2.7). This behavior is similar in all samples.

There is a distinct magnetic behavior for the two structural phases, revealed by the change of shape of the isothermal magnetization curves, Figure (2.6). The visible crossing of the isothermal magnetization curves, at 1.5 T for sample 1 and 1.2 T for all other samples, reveals different magnetic anisotropies between the martensitic and austenitic phases. Above T_M the magnetization reveals a softer ferromagnetic behavior, easily reaching its saturation magnetization. Below this temperature, however, the saturation magnetization is reached much slower and its value is higher, indicating either an increase of the magnetic anisotropy, when going from the martensitic to the austenitic phase, or a change in the easy-direction of the magnetization [22].

The behavior described above is also reflected in the magnetization curves as a function of temperature, as seen in Figure (2.7). There we can see that for curves corresponding to low fields (below 1.5 T in sample 1 and 1.2 T for all other samples), for increasing temperature around T_M, the magnetization increases, while for high fields

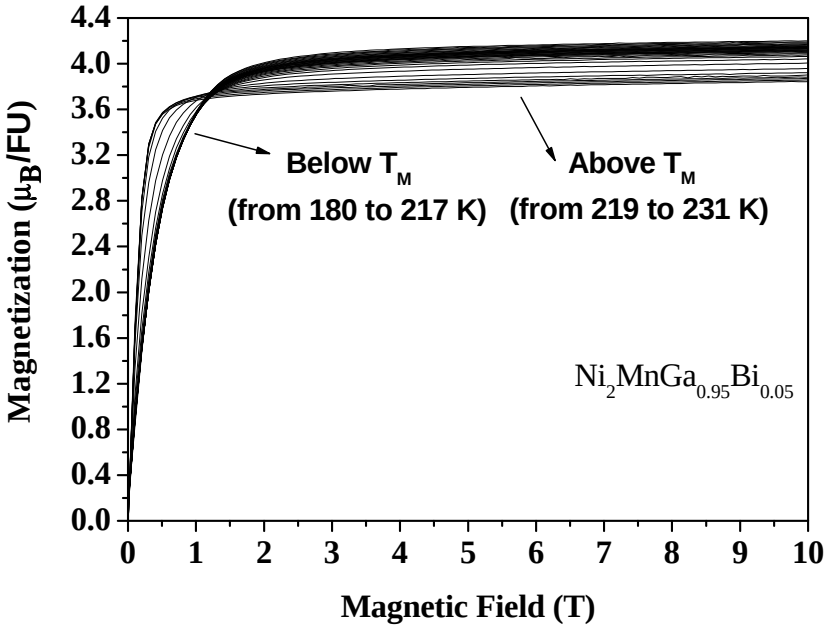

Figure 2.6: Magnetization vs applied magnetic field for sample 4 (5% of Bi) around the structural transition revealing two distinct magnetic behaviors for the two structural phases.

the magnetization actually decreases. For fields closer to the isotherm crossing there is a very small magnetization jump around T_M.This is easily understood by observing Figure (2.6); before the isothermal crossing (below 1.5 T for sample 1 and 1.2 T for all other samples), for equal values of magnetic field, we find that they display a growing magnetic moment, reflected in Figure (2.7) as a jump in the magnetic moment at TM for curves corresponding to low field values. After the isothermal crossing however, as temperature increases, for the equal magnetic field values, the isotherms display a gradual decrease of magnetic moment, as they have invert their positions relatively to one another, reflected in Figure 3 as the visible fall of magnetic moment for 2 T, 4 T and 10 T.

Knowing that the magnetic entropy change (ΔS) is given by equation (1.2), the previously described magnetic behavior will obviously have repercussions in the magnetic entropy change. This is shown in Figure (2.8).

The maximum value of ΔS increases up to 1.2 T, where there is the crossing of the isothermal magnetization curves. This behavior is similar in samples 2, 3 and 4. In sample 1, as already mentioned, the isothermal curves crossing occurs at 1.5 T, being that the applied field where we will find the maximum magnetic entropy change. This result is expected because ΔS is a function of the area between magnetic isotherms.Before the isotherm crossing we have a positive area between isotherms, creating the positive ΔS, after the crossing, as the isotherms invert their positions, the

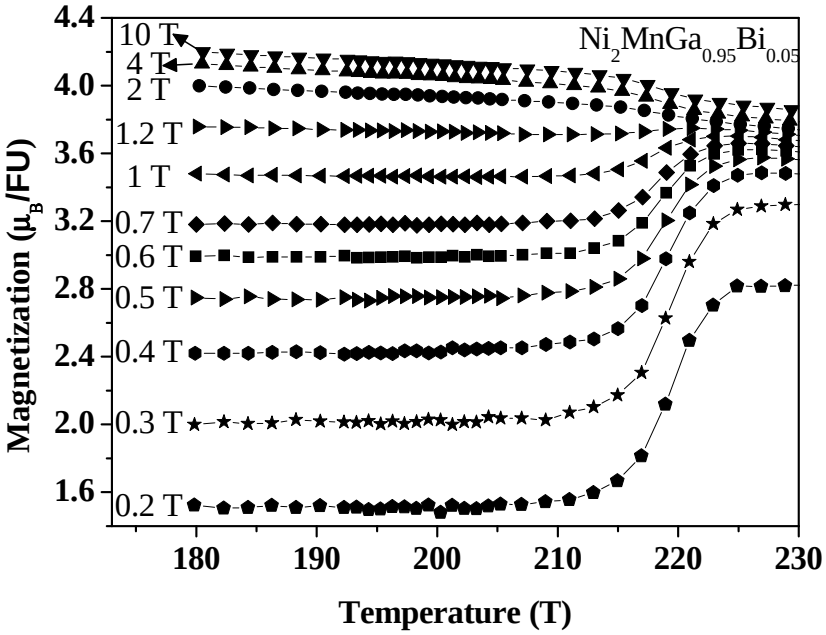

Figure 2.7: Magnetization vs temperature for sample 4 around the structural transition temperature revealing the change in the magnetization slope for various magnetic fields. As the sample's magnetization for high fields above T_M is lower that below, due to the magnetic anisotropy of the two structural phases, we measure a decrease in the value of magnetization, whereas for low fields we measure an increases.

area between them becomes negative, reflecting in the decrease and eventual negative value of ΔS.As we increase the magnetic field change there will be a decreasing of the maximum magnetic entropy change and only at 8 T for sample 1, 7.3 T for sample 2 and 6.2 T for samples 3 and 4 both areas (above and below the crossing of magnetization curves), are balanced, and, consequently, the magnetic entropy change is zero.

By monitoring the maximum values of the magnetic entropy curves for all four samples for several applied magnetic fields we obtain therefore the Figure (2.9). We can clearly see the increase in the maximum peak value, reaching its maximum around 1.5 T for sample 1 and 1.2 T for all the other samples, which steadily decreases from this value on. From this result we can conclude that the use of the stoichiometric alloy for magnetic cooling purposes around the structural transition is limited to the use of fields below 1.5 T, having its maximum entropy variation value of about 3.8 J/Kg.K; any field above this value will in fact reduce its magnetocaloric power.

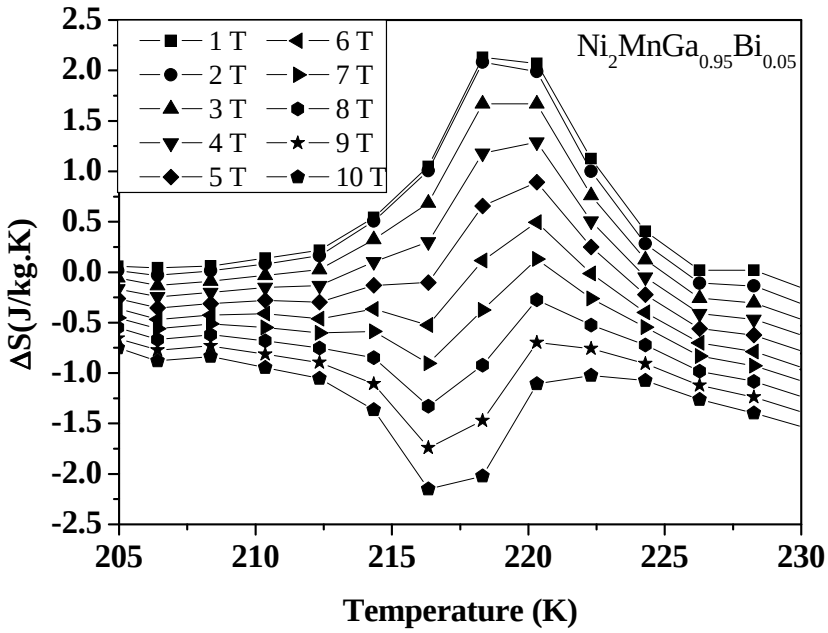

Figure 2.8: Magnetic entropy variation vs temperature for sample 4 for various values of applied magnetic field. As the magnetic isotherms invert their positions relatively to one another, according to equation 1.2, after the isothermal crossing the value of ΔS will start to decrease.

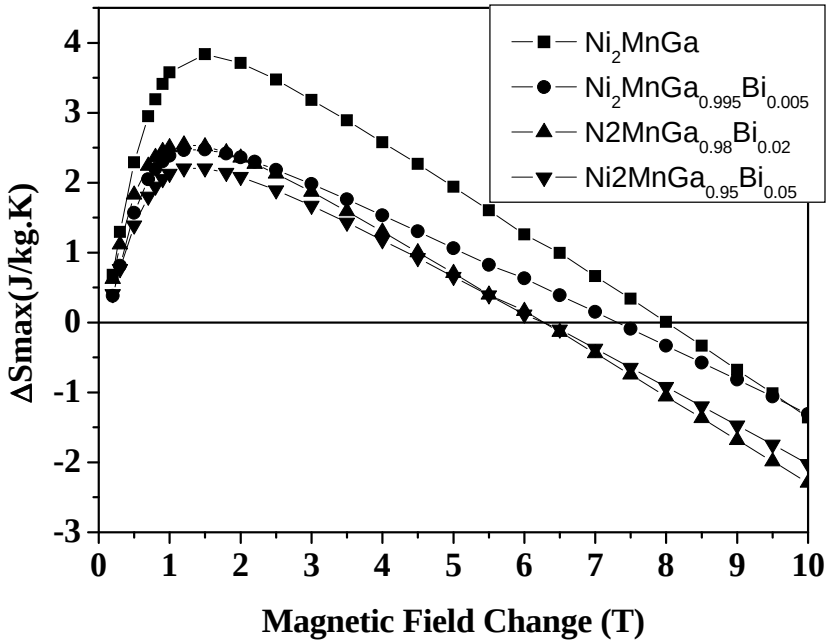

Figure 2.9: Maximum magnetic entropy change as a function of applied field change, for all samples. The value of ΔS increases as the magnetic isotherms crossing field is reached, after this point, due to the magnetic anisotropy of the two structural phases, ΔS steadily decreases. All alloyed samples present a much lower value of ΔS.

Chapter 3

$PrNi_{5-x}Co_x$ hard magnet alloys

The pseudo-binary $PrNi_{5-x}Co_x$ compounds are derived from the parents $PrCo_5$ and $PrNi_5$ compounds. The Co rich side is especially interesting due to its high Curie temperature (higher than Nd-Fe-B magnets) [58]. The $PrNi_5$ compound is paramagnetic due to the high crystal field of this compound [59]; however, it has been successfully used for cooling at very low temperatures through the adiabatic demagnetization process [60].

For intermediate concentrations of x, some authors [61–64] found for $RNi_{5-x}Co_x$ compounds (R: rare earth), that for increasing Co content there is a monotonic increasing of T_C and M_S, an abrupt change of T_C and M_S, as function Co content near x=2.0, and a discontinuity in lattice parameters also around x=2.0. Some of these compounds $RNi_{5-x}Co_x$ also present a strong magnetocrystalline anisotropy and, consequently, some families show a spin reorientation process [65].

As such, we prepared samples of the $PrNi_{5-x}Co_x$ series with small compositional increment (δx=0.05), belonging to the special compositional region between x=2 and x=3 in order to perform a detailed analysis of its magnetic, structural and magnetocaloric properties. Furthermore, we have chosen the praseodymium rare earth because $PrNi_5$ is the only compound, among those RNi_5, that is paramagnetic [66], and therefore this series, $PrNi_{5-x}Co_x$, is the richest one from the magnetic point of view.

The author of the current report did not participate in the preparation or characterization of this alloy, only in the consequent data analysis. The main researcher of the current alloy is Dr. D. L. Rocco [67].

3.1 Experimental Procedure

3.1.1 Sample Preparation

Similarly to the $Ni_2MnGa_{1-x}Bi_x$ series, the $PrNi_{5-x}Co_x$ (x = 1.95, 2.07, 2.15, 2.20 , 2.25, 2.30, 2.40, 2.45, 2.50, 2.55 and 3.00) samples were prepared in a Buhler arc melting furnace, at IFIMUP-University of Porto , with the appropriate amount of constituent elements namely, praseodymium (99.9%), nickel (99.995%) and cobalt (99.995%). The furnace works with a water-cooled copper crucible and was pre-evacuated better than $2x10^{-6}$ mbar and refilled with high-purity argon gas. The samples were re-melted up to three times to ensure homogeneity and then annealed in an evacuated quartz tube at 1020 K for 7 days, with a subsequent quench in liquid nitrogen. The weight loss was $< 0.5\%$.

3.1.2 Crystallography and structural characterization

1º - X-ray diffraction

X-ray diffraction analysis was performed at the University de Trás-os-Montes e Alto Douro (UTAD) using a multichannel x-ray diffractometer from Phillips with a Cu and Kα radiation. From Rietveld-type analysis we could ratify that the annealed samples are single phase, at least within the X-ray resolution, i.e., possible impurity phase is lower than 5% vol, and confirm that those crystallize in the hexagonal $CaCu_5$(P6/mmm) type structure and the lattice parameters (at 300 K) are in good agreement with values found by Chuang *et al* [62] and Andreyev *et al* [63] for poly- and single crystals, respectively.

2º - Energy dispersive x-ray spectroscopy EDS

In order to check homogeneity and stoichiometry of the samples, energy dispersive x-ray spectroscopy (EDS) technique was used, more precisely the Phillips-FEI/Quanta 400, from UTAD. We could verify that the samples, after annealed, are single phase and, in addition, show a composition of the elements within 6% of the nominal value.

3.1.3 Magnetic measurements

Magnetization as function of magnetic field and temperature were carried out in two vibrating sample magnetometer (VSM), one for low temperature (up to 300 K), at the University of Aveiro, and another for measurements at high temperature (300 K up to

900 K) at IFIMUP-University of Porto. Some measurements were also done in SQUID magnetometer also at IFIMUP-University of Porto.

3.2 Magnetic properties

From the samples studied by the author (with x corresponding to 1.95, 2.15, 2.2, 2.25, 2.3 and 3.0, below 300 K) we measured the M(H), Figure (3.1). These magnetic isotherms were measured with constant temperature values from 100 K to 307 K, with an increment of 3 K between 100 and 181 K and an increment of 6 K between 181 and 307 K. Then using the appropriate Matlab routine created by Dr. Mário Reis, calculated M(T), Figure(3.2).

As it is easily observed in Figure (3.1) there occurs a crossing of the magnetic isotherms off of the point of origin (0,0). This does not translate any kind of magnetic behavior, but rather the influence of the demagnetization field or some remanet magnetic field left in our coils between measurements. This, of course, will have some impact on our calculated M(T) graphs, as it is observed in the low field curves of Figure (3.2).

Also, we can observe the influence of the amount o Co in the maximum Magnetization in Figure (3.3).

Following a similar procedure to $Ni_2MnGa_{1-x}Bi_x$ series, using equation (1.2) we obtained ΔS for these samples, displayed in Figure (3.4)

The peaks displayed in Figure (3.4) do not correspond to the magnetic transition around T_C or another widely studied magnetic process, but rather to a spin reorientation process.

3.2.1 Competing magnetic anisotropies and the spin reorientation process

To understand this phenomenon as it occurs in this particular alloy we have to analyze the crystal structure of the alloy. See in Figure (3.5) the crystal structure.

As it is easily observed, there are two Co\Ni sites (3g and 2c-Wyckoff symbols) and only one Pr site (1a). If we initially consider a $PrNi_5$ alloy, as we start adding Co to the lattice it will preferentially occupy the 2c sites [69, 70], until it reaches a critical concentration ($x_c \sim 1.9$), until this point there is a linear increase in T_C, all the 2c sites are fully occupied and the Co is isolated in laminar clusters.

If we continue to add Co it will now start to fill the 3g sites, previously occupied by Ni. This means that the previously isolated Co clusters will begin to have interaction

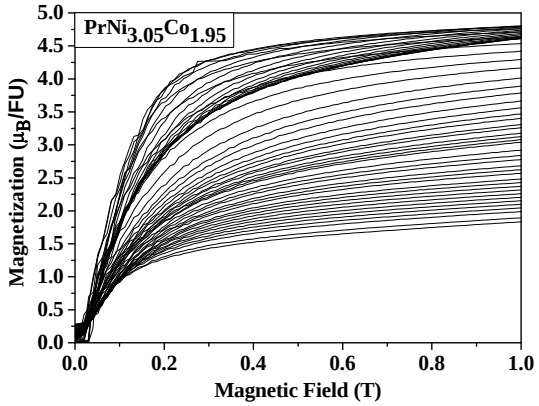

(a) Magnetization vs applied magnetic field for the $PrNi_{3.05}Co_{1.95}$

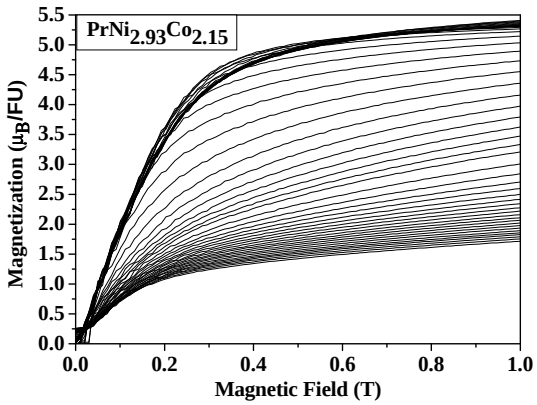

(b) Magnetization vs applied magnetic field for the $PrNi_{2.85}Co_{2.15}$

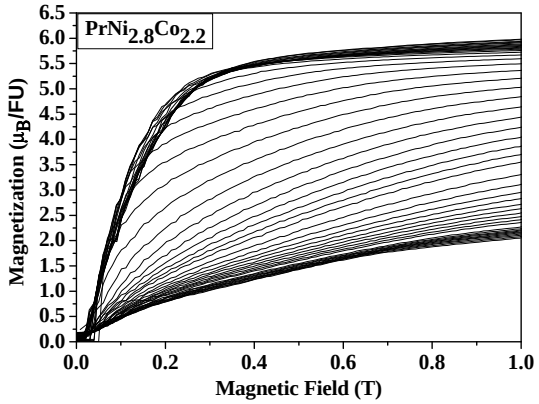

(c) Magnetization vs applied magnetic field for the $PrNi_{2.8}Co_{2.2}$

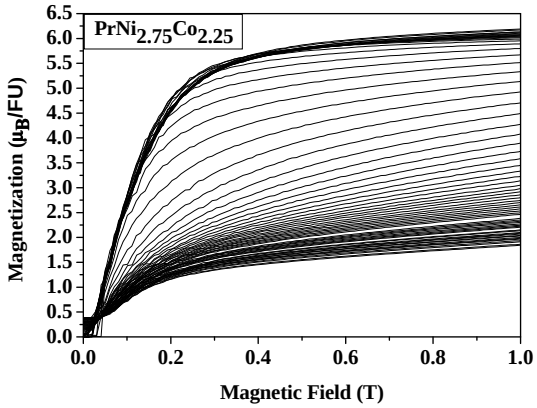

(d) Magnetization vs applied magnetic field for the $PrNi_{2.75}Co_{2.25}$

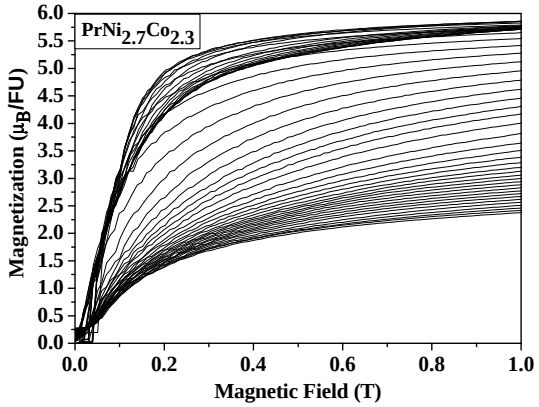

(e) Magnetization vs applied magnetic field for the $PrNi_{2.7}Co_{2.3}$

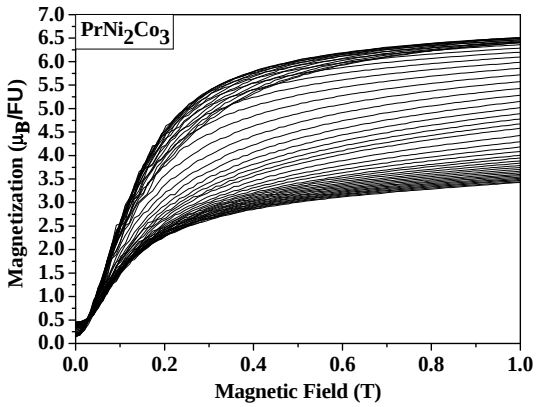

(f) Magnetization vs applied magnetic field for the $PrNi_2Co_3$

Figure 3.1: Magnetization vs applied magnetic field for the samples studied by the author, for temperatures below 300 K

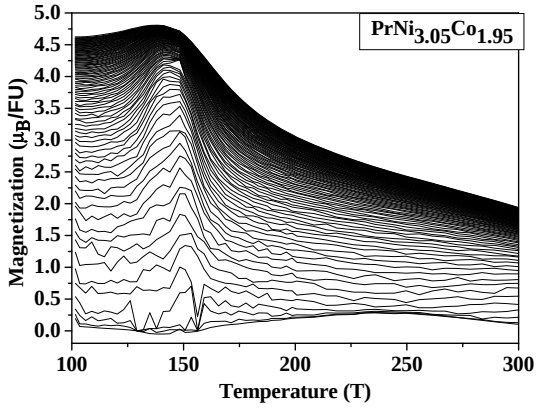

(a) Magnetization vs temperature for the $PrNi_{3.05}Co_{1.95}$

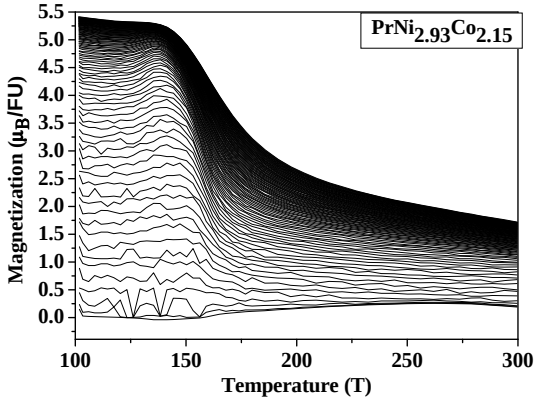

(b) Magnetization vs temperature for the $PrNi_{2.85}Co_{2.15}$

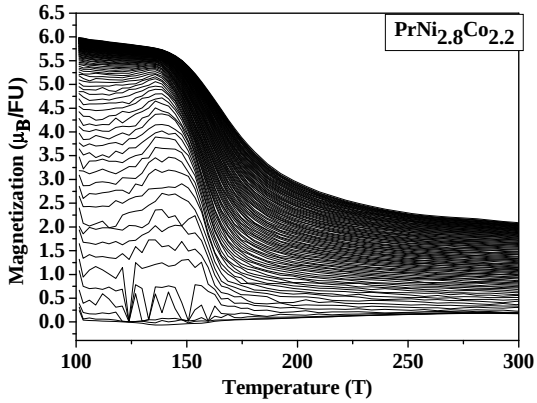

(c) Magnetization vs temperature for the $PrNi_{2.8}Co_{2.2}$

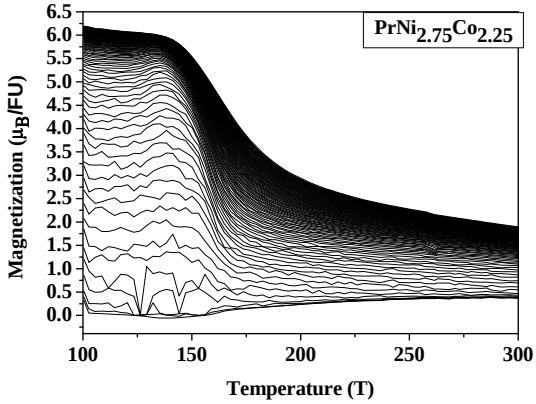

(d) Magnetization vs temperature for the $PrNi_{2.75}Co_{2.25}$

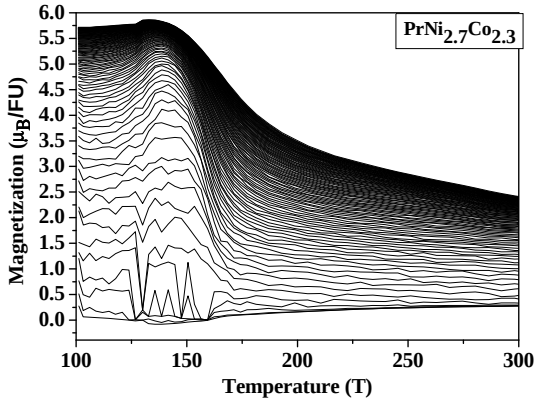

(e) Magnetization vs temperature for the $PrNi_{2.7}Co_{2.3}$

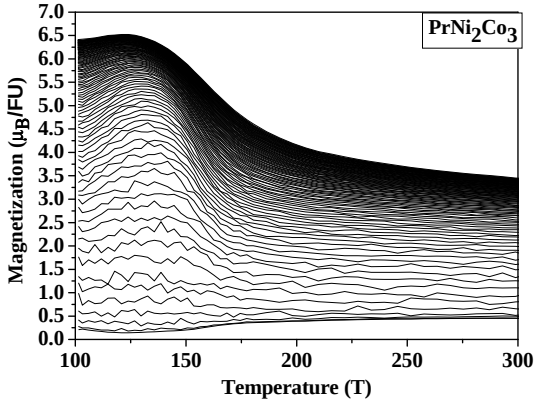

(f) Magnetization vs temperature for the $PrNi_2Co_3$

Figure 3.2: Calculated magnetization vs temperature for the samples studied by the author, with applied magnetic fields between 0.01 and 1 T, with an increment of 0.01 T

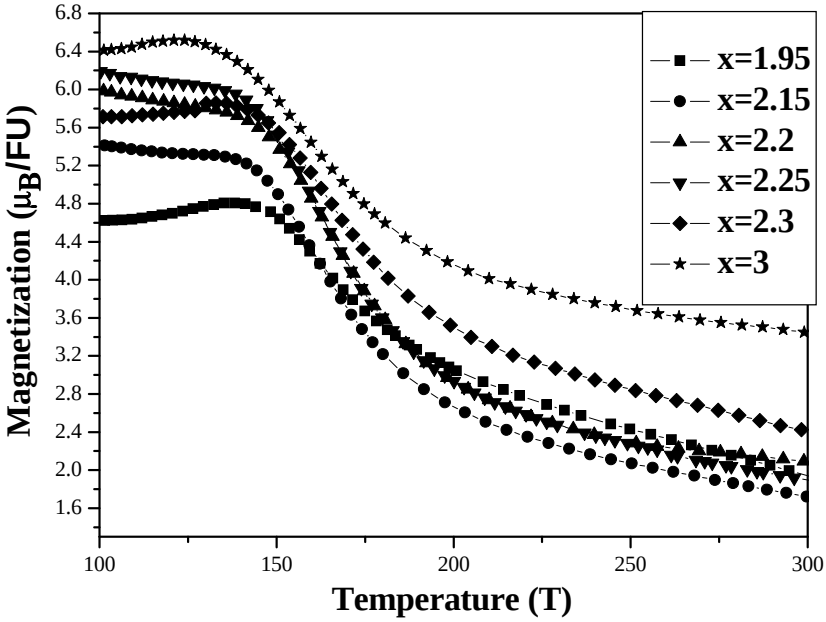

Figure 3.3: Magnetization vs temperature for all the samples studied by the author for 1 T

with each other, greatly increasing T_C. This is known as a percolation process.

This information, combined with previous information from the literature [63] enabled us to build a magnetic phase diagram for the $PrNi_{5-x}Co_x$ series , as presented in Figure (3.6).

In Figure (3.6) we can observe the previously stated concentration of x$\sim$1.9, up to which T_C increases linearly and above which there is a great increase in T_C corresponding to a percolation process [71].

Knowing that rare-earth ions with α_J<0 (Pr, Nd, Tb, Dy and Ho) tend to have an easy magnetization direction in the basal plane (a-b plain) of the hexagonal structure, and that the Co sublatice anisotropy is aligned along the c-axis, we have a strong competition of magnetic anisotropies in this alloy [72]. This competition induces therefore a spin reorientation phenomenon in these compounds and rules some of the magnetic properties of these materials.

For low temperature, increasing Co content, the total magnetic moment lies in the a - b plane up to x $\sim$ 3.5 (estimated value from [63], half-filled up-triangle symbols). Above this concentration the total magnetic moment changes to the cone configuration. It is easy to understand, because the magnetocrystalline anisotropy of Co sublattice increases due to an increasing of Co content and therefore its anisotropic energy is comparable to that of the Pr sublattice. On the other hand, increasing temperature for concentrations below $x_c \sim 1.90$ the system changes from the ferromagnetic order to a paramagnetic one. Note that substitution of Co into $PrNi_5$ (paramagnetic) leads to a

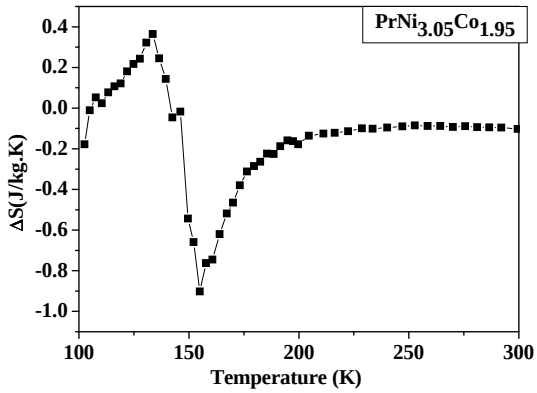

(a) Magnetic entropy change for the $PrNi_{3.05}Co_{1.95}$

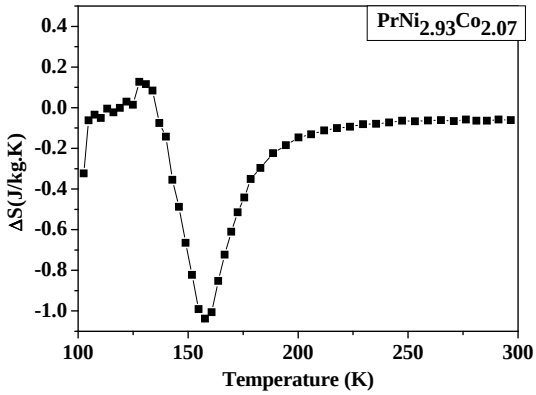

(b) Magnetic entropy change for the $PrNi_{2.85}Co_{2.15}$

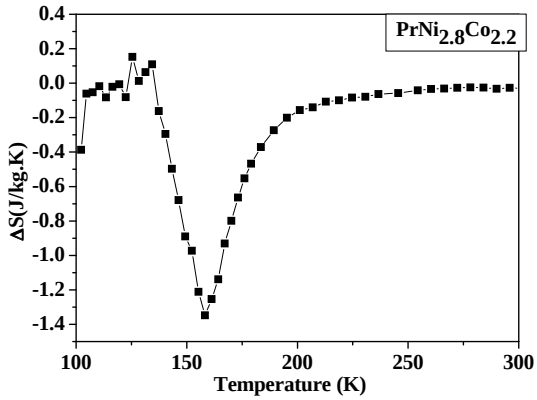

(c) Magnetic entropy change for the $PrNi_{2.8}Co_{2.2}$

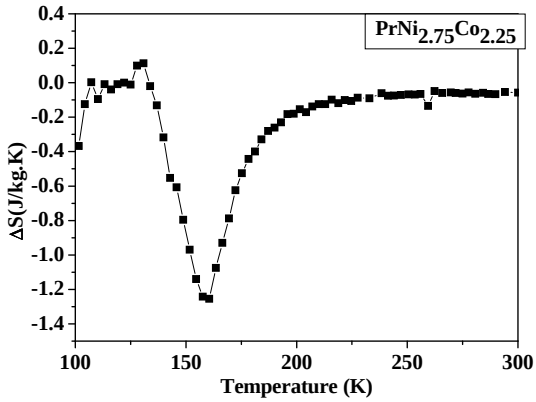

(d) Magnetic entropy change for the $PrNi_{2.75}Co_{2.25}$

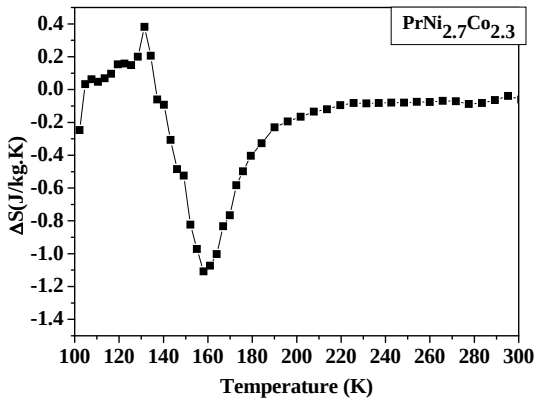

(e) Magnetic entropy change for the $PrNi_{2.7}Co_{2.3}$

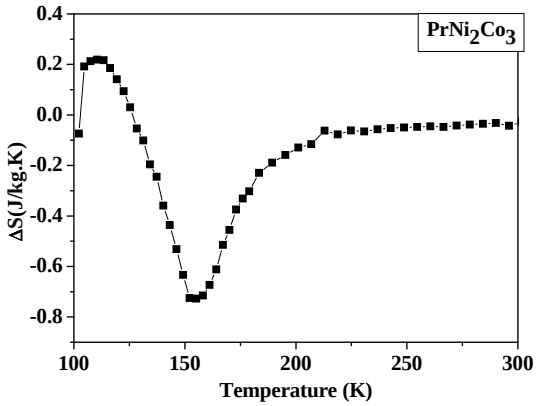

(f) Magnetic entropy change for the $PrNi_2Co_3$

Figure 3.4: Magnetic entropy change for all the samples studied by the author, for temperatures below 300 K and applied magnetic field of 1 T

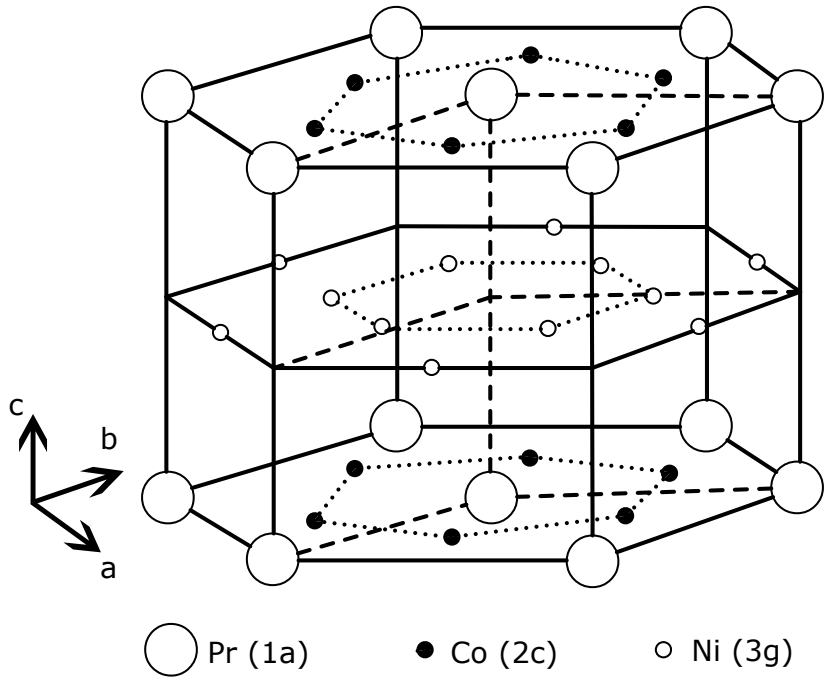

Figure 3.5: Representation of the $CaCu_5$-type structure (taken from [68]) for the $PrNi_3Co_2$ compound. The Co atoms preferentially occupy 2c sites rather than the 3g sites [69].

linear (and slow) increase of the Curie temperature, changing from zero (for x = 0) up to 60 K (for $x_c \sim 1.90$). This is reasonable, because the critical temperature in these compounds is mainly ruled by Co-Co interaction and therefore Co substitution in the Ni site increases the overall Co-Co exchange interaction which leads to an increasing of T_C. Above this critical concentration, up to x $\sim$ 3.5 (estimated value), still considering a temperature increase, we can find T_{SR1}, where the total magnetic moment changes from the a - b plane to the cone arrangement, and then T_{SR2}, where the total magnetic moment changes from the cone configuration to axial arrangement (c-axis). Further increasing of temperature reaches the Curie temperature. Above x $\sim$ 3.5 the system at zero temperature has the total magnetic moment in the cone position and then changes at T_{SR2} to an axial configuration. Again, further increasing of the temperature lead to a Curie temperature.

This conclusion is confirmed by measurements of magnetization as a function of temperature (for a applied magnetic field value of 0.2 T) for sample $PrNi_{3.05}Co_{2.95}$, Figure (3.7), this behavior in analogous in all other samples. There we can clearly see the inflections corresponding to T_{SR1} and T_{SR2}. T_C however is only found at much higher temperatures, having a dependence with the Co content.

As such, for both T_{SR1} and T_{SR2}, the spin reorientation temperatures, we will have an associated magnetic entropy change, resulting in the two peaks we observed in

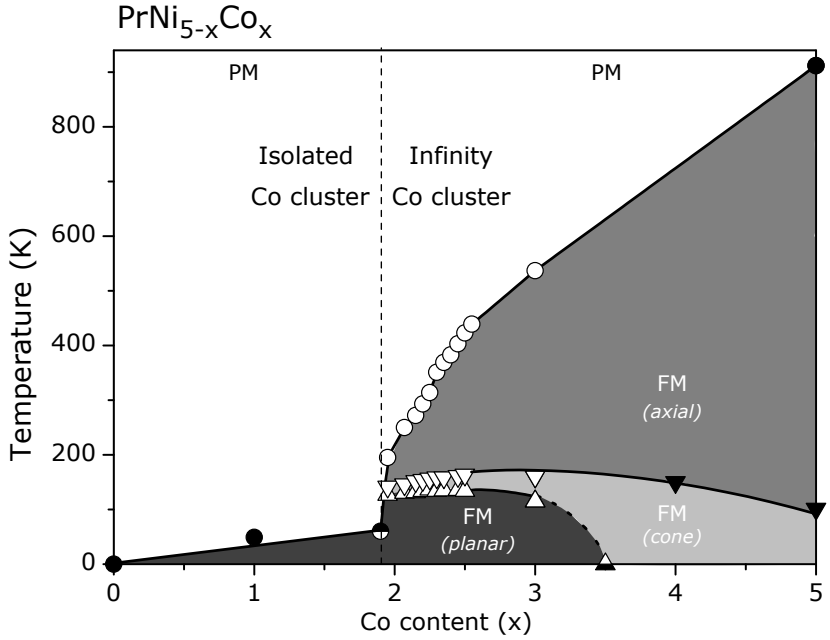

Figure 3.6: Magnetic phase diagram of the $PrNi_{5-x}Co_x$ system. Open symbols - work performed by the Magnetocaloric group of the University of Aveiro, closed symbols - Andreyev et al [63] and half filled symbols - estimative. ○ and ● - Curie temperature, △ and ▲ - T_{SR1} (the total magnetic moment changes from the basal plane to the cone arrangement) and ▽ and ▼ - T_{SR2} (the total magnetic moment changes from the cone arrangement to c-axis). Finally, FM stands for ferromagnetic and PM for paramagnetic.

Figure (3.4).

3.3 Advantages of the Spin Reorientation to The Magnetocaloric Effect

When we combine the results of ΔS obtained by the author with those already studied by Dr. D. L. Rocco, for a below and above 300K we then obtain Figure (3.8).

It is interesting to notice that the maximum at T_{SR2} is larger than that at T_C. This is ascribed to the fact that the magnetization around the spin reorientation from cone to axis has a sharper change than that around the para-ferromagnetic transition, as shown in Figure (3.7) and consequently equation (1.2) will give us a much higher value. In addition, spin reorientation processes are accompanied by a magnetostriction effect along the c axis [63, 70], increasing therefore the magnetocaloric potential.

Let us focus our attention to the x = 3.0 sample (top panel of Figure (3.8). As the previous case, the maximum magnetic entropy change around T_C is smaller than that around T_{SR2}. However, it is worth to note the full width at half maximum δT_{FWHM}

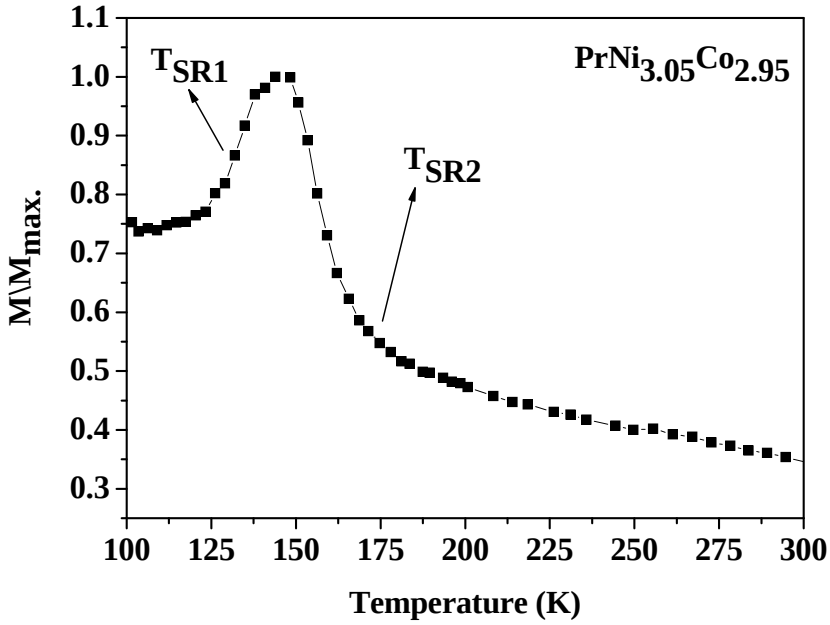

Figure 3.7: Normalized magnetization as a function of temperature for the $PrNi_{3.05}Co_{2.95}$ sample for an applied field of 0.2 T.

around $T_C = 537$ K, reaching 88 K (for 10 kOe), whereas around $T_{SR2} = 202$ K we found $\delta T_{FWHM} = 34$ K. From the phase diagram it is expected that the peaks related to T_{SR1} and T_{SR2} do not change in temperature, while we can expect a strong temperature dependence of the peak associated to T_C. Decreasing Co content, we found the sample with T_C around room temperature, that is for x $\simeq$ 2.2. Further decreasing of Co content induces a merging of the magnetic entropy change peaks, i.e., that around T_C and around T_{SR2}. The onset concentration for this merged peaks occurs in between 2.07 $<$ x $<$ 2.15 and drastically increases the full width at half maximum δT_{FWHM} of both peaks, as shown in Figure (3.9) (bottom panel).

Concerning the maximum magnetic entropy change ΔS around T_C, it remains approximately constant through Co changes; and, on the other hand, ΔS_{max} around the spin reorientation has a strong dependence upon Co substitution with a maximum at x $\sim$ 2.5 (see Figure (3.9)-top panel). The Relative Cooling Power (RCP), defined as ΔS_{max} times δT_{FWHM}, is quite large for our compounds, in spite of this low value of magnetic field change (10 kOe). Calculated RCP for the sample with both peaks merged (x = 2.07, for instance), reaches 30 Jkg^{-1}, whereas this quantity for metallic Gd is 60 Jkg^{-1}, at the same conditions [73]. This is worthy to note that the RCP of the Gd is only 2 times larger than $PrN_{5-x}Co_x$ while the maximum ΔS_{max} is 12 times bigger.

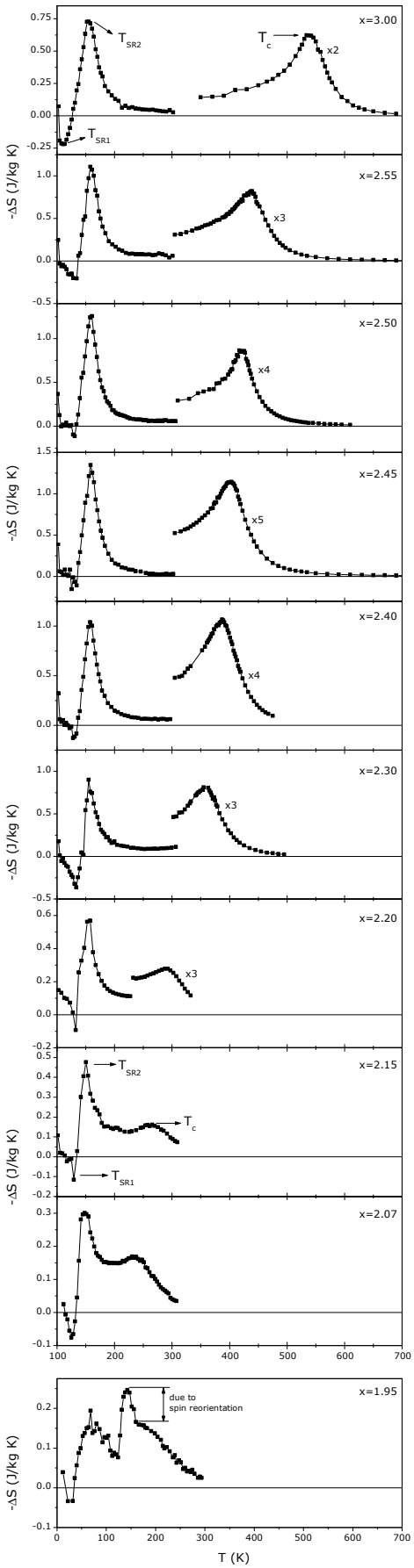

Figure 3.8: Magnetic entropy change obtained from the magnetization as a function of magnetic field for all of the samples prepared. Those peaks are associated to the spin reorientation process (around T_{SR1} and T_{SR2}) and T_C. Note the high value of δT_{FWHM} of peak around T_C (for higher Co concentration). Decreasing Co content the peaks around T_{SR2} and T_C merge increasing the δT_{FWHM}.

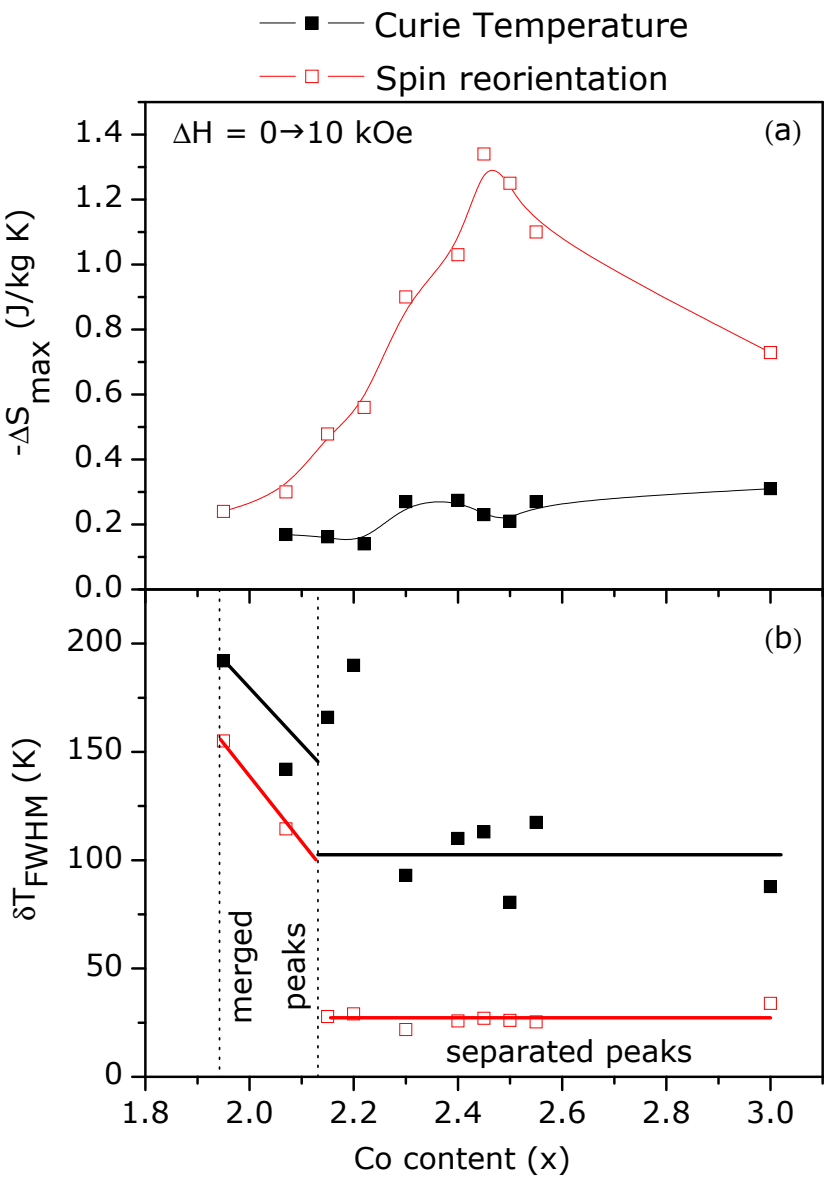

Figure 3.9: (a) Maximum magnetic entropy change around T_C and T_{SR2}. (b) Full width at half maximum around T_C and T_{SR2} peaks. Below x = 2.15 those peaks merge, increasing the δT_{FWHM}.

Chapter 4

RNi_2 alloy

The study of these alloys was performed in the context of a collaboration of the Magnetocaloric Group of the University of Aveiro with Pedro J. von Ranke's group at the Universidade do Estado do Rio de Janeiro as a continuation of their previous work [32].

In their cited article P. J. von Ranke *et al* studied the magnetocaloric proprieties of the RNi_2 series (R= Nd, Gd, Tb, Ho, Er), in which the CEF anisotropy plays a fundamental role, using a theoretical Hamiltonian model that includes the exchange interaction in molecular-field approximation and the Zeeman effects, comparing their results with experimental ones.

As such, our part in this work was mainly to produce the RNi_2 samples (R = Nd, Gd, Tb), study their homogeneity and evaluate the magnetocaloric effect so as to compare it with the theoretical results.

4.1 Experimental Procedure

4.1.1 Sample Preparation

RNi2 (R= Nd, Gd, Tb) samples were prepared in a Buhler arc melting furnace, at IFIMUP-University of Porto in a purified argon atmosphere starting from the appropriate amounts of the constituent elements, namely 99.9% for all the rare earths and 99.995% for the Ni. No loss of mass was observed after the fusion. To ensure homogeneity the ingots were sealed in vacuumed quartz tubes and underwent heat treatment for 14 days at 900 K.

4.1.2 Characterization

1º - X-ray diffraction

This analysis was performed at the University de Trás-os-Montes e Alto Douro (UTAD) using a multichannel x-ray diffractometer with a Cu and Kα radiation. Then, using the refinement procedure of the PowderCell software the crystal structure and lattice parameters were analyzed.

2º - Magnetic measurements

Magnetization as function of magnetic field and temperature were carried out in a vibrating sample magnetometer (VSM), up to 300 K in the University of Aveiro only for the $GdNi_2$ sample, all other samples were measured in the Universidade Federal do Rio de Janeiro by one other collaborator, Dr. Angelo Gomes.

4.2 Results and Discussion

4.2.1 X-ray diffraction

X-ray diffraction with Rietveld refinements reviled that the $TbNi_2$ and $GdNi_2$ samples were monophasic ($TbNi_2$ had some minor pure Tb segregation), while the $NdNi_2$ samples presented two other phases: $NdNi_3$ (22% of the sample mass) and Nd_6O_{11} (14% of the sample mass), most probably due to an unsuccessful vacuuming of the quartz tubes that gave rise to the presence of oxygen in the samples.

All these results can be observed in Figure (4.1) and are summarized in Table (4.1)

Table 4.1: RNi_2 phases

(a) $TbNi_2$		
Phase	% volume	% mass
$TbNi_2$	99.8	99.82
Tb	0.2	0.18
(c) $NdNi_2$		
Phase	% volume	% mass
$NdNi_2$	61.6	63.7
$NdNi_3$	20.9	21.9
Nd_6O_{11}	17.5	14.4
(d) $GdNi_2$		
Phase	% volume	% mass
$GdNi_2$	100	100

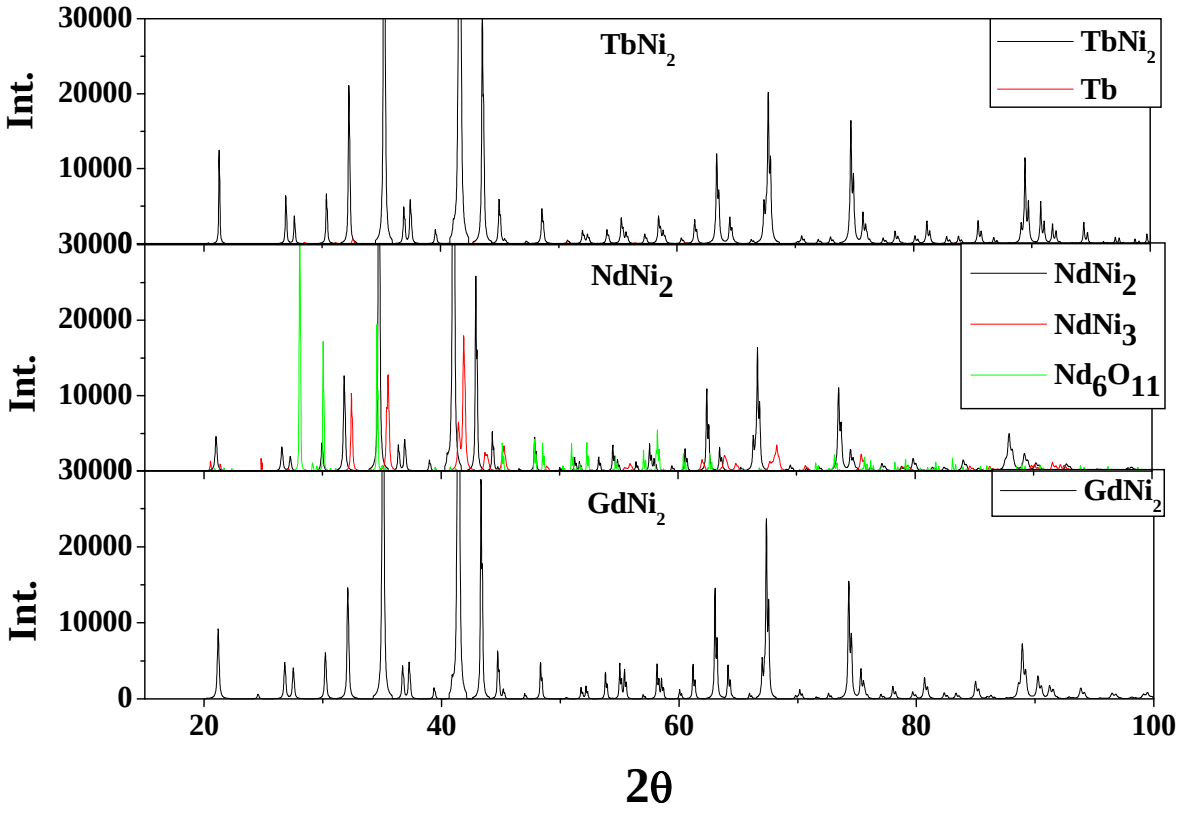

Figure 4.1: X-ray diffraction of all RNi_2 samples

Monitoring of the lattice parameter of all four samples revealed an increase in a as we go down the periodic table, this is expected and is due to the phenomenon known as lanthanide contraction, which consists in the decrease of the ionic radios of the lanthanide family with the increases of the electronic number. These result may be observed in Figure(4.2).

This effect rises from the fact that in lanthanides as the 4f sub shells are being filled with more electrons they become less and less capable of shielding the electrons form the outer (5^{th} and 6^{th}) shells from the attraction of the nucleus. As such the shielding effect of the inner shells is less able to counter de decrease of the ionic radios caused by the increasing nucleus charge.

4.2.2 Magnetic measurements

Using Equation (1.2) we obtained the value of the magnetic entropy change as a function of temperature for all samples.

It is important to take into consideration that, for the $NdNi_2$ sample, the entropy change was adequately normalized by the mass of the phase we wished to study, even thought secondary phases present in this sample were not ferromagnetic [74], their

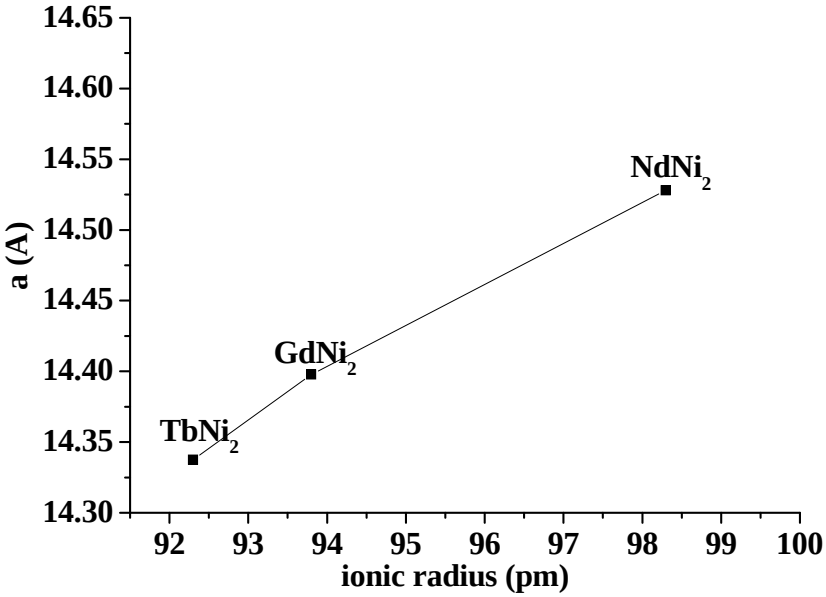

Figure 4.2: Lattice parameter vs the ionic radius for all four samples, revealing the lanthanide contraction.

presence in the sample still influences the value of ΔS for the paramagentic phase and as such we can only consider our results to be a rough approximation.

As such, in Figure (4.3) we can observe ΔS for all three samples. The theoretical values presented are the ones already published by Pedro J. von Ranke *et al* [32].

We can see that the theoretical Hamiltonian model used by Pedro J. von Ranke's team was very successful at predicting the magnetocaloric behavior of the $GdNi_2$ and $TbNi_2$ samples. The $NdNi_2$ sample however, has only 63% of the interesting phase, but making the appropriate correction the experimental measurement, seeing as the secondary phases aren't magnetic, it came close to the theoretical.

The ΔS values may be seen in Table (4.2)

Table 4.2: Summary of the magnetization and entropy variation information regarding the RNi_2 series

	pure phase	-ΔS (J/mol.K) theor.	-ΔS (J/mol.K) meas.
$GdNi_2$	$\surd$	3.55	3.33
$NdNi_2$	$\times$	3.93	2.18
$TbNi_2$	$\surd$	6.94	4.17

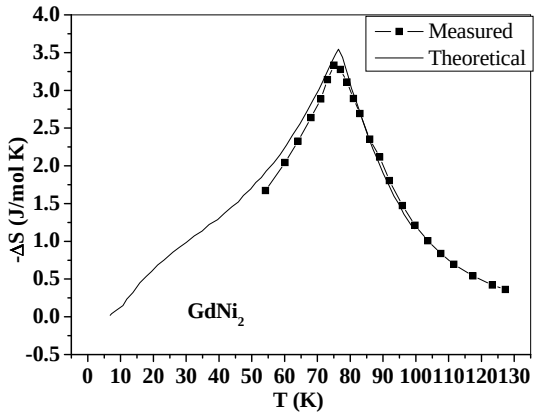

(a) $GdNi_2$ magnetic entropy change in J/mol.K

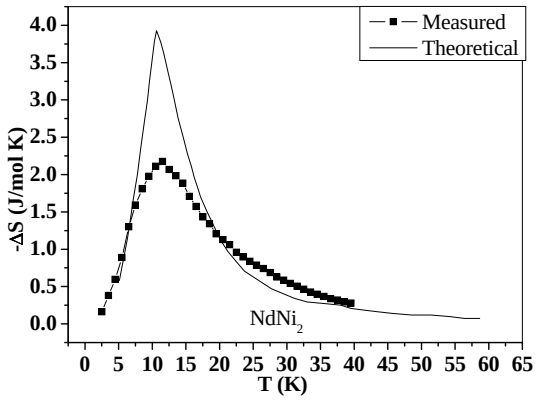

(b) $NdNi_2$ magnetic entropy change in J/mol.K

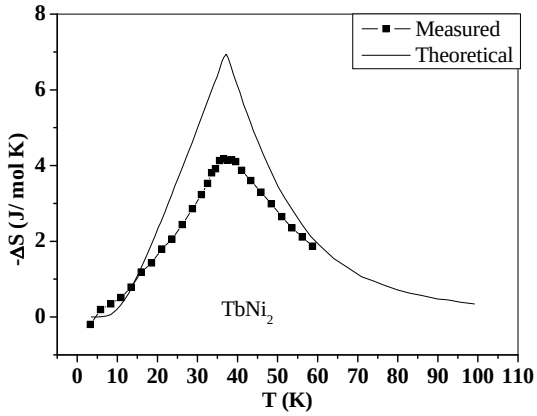

(c) $TbNi_2$ magnetic entropy change in J/mol.K

Figure 4.3: ΔS for all RNi_2 samples for magnetic field change of 5 T

Chapter 5

Conclusions and Future Work

5.1 $Ni_2MnGa_{1-x}Bi_x$ alloy

Taking advantage of the Heusler alloy's high composition sensitivity, we produced four different samples with different percentages of Bi in an attempt to merge the structural and magnetic transition temperatures for magnetocaloric purposes. We also aimed to see the influence of the magnetic anisotropy and the magnetocaloric effect of the compounds.

For our alloyed samples we observed an increase in T_M and a decrease in T_C, as was our objective, making the Bismuth alloying a promising method to possibly merge the two transitions and possibly generate a giant magnetocaloric effect near room temperature. These results were due to the increase in e/a which has been shown to be associated with changes in T_M and T_C. Also, the substitution of Ga for Bi in our alloyed samples has caused an increase in the lattice parameter a in some areas of our samples, resulting in an increase of the distance between Mn atoms and a consequent decrees of the magnetic transition T_C.

However, we measured a much smaller value of the ΔS maximum than expected, 2.2 J/kg.K at 1.2 T. This, despite the previous conclusion, compromises their use for magnetic refrigeration purposes. As such, these results point to the obvious continuation of the study of Bismuth alloying of the Ni_2MnGa alloy, to see how far it is possible for T_M and T_C to come close using this method.

For our pure Ni_2MnGa sample (sample 1) we have found that its use for magnetic cooling purposes around the structural transition is limited to fields below 1.5 T. This is due to the fact that the two structural phases have very different anisotropies. The martensitic phase (below $T_{M)}$ has a much higher saturation magnetization than the austenitic phase (above T_M), as such their magnetic isotherms cross at the mentioned field of 1.5 T (1.2 T for the alloyed samples), as ΔS is calculated as a function of the

area between magnetic isotherms, this behavior causes an inversion in the signal of ΔS. As such we have a maximum magnetic entropy variation value of about 3.8 J/kg.K, any field above the previously stated, beyond the isothermal crossing, will in fact reduce its magnetocaloric power. The same conclusion is applied to the Bi substituted samples.

The syntherization treatment has shown to be very effective in preventing the undesired result of Bi segregation in the Ni_2MnGa alloy, and therefore we will use this treatment to try to produce samples with much higher Bi concentration. In fact we have already started the production of six new $Ni_2MnGa_{1-x}Bi_x$, with x=0;0.002;0.1;0.25 and 0.5. The sixth sample, contrary to the other six which were produced with the appropriate amounts of the constituting elements, has been made with the an amount of a pre-alloyed MnBi sample, as to produce the stoichiometry $Ni_2MnGa_{0.9}Bi_{0.1}$.

5.2 $PrNi_{5-x}Co_x$ alloy

In the present work we prepared a large set of samples with a small compositional increments ($\delta x \sim 0.05$) within the special concentration range $2 < x < 3$ of the $PrNi_{5-x}Co_x$ series. Although the participation of the author of the current report was rather reduced considering the bulk of this study, the joint efforts of the Magnetocaloric group, and Dr. D. L. Rocco in particular, could establish the following conclusions refereing to this series.

It is well established [72] that the competition between the anisotropy energy of Pr sublattice (that tend to align the magnetic moment in the basal a - b plane) and Co sublattice (that, on the contrary, tends to align the magnetic moment along the c-axis), leads to a spin reorientation process. In this sense, this series has a rich phase diagram, which, with information from previous literature could be determined. In addition to the spin reorientation temperatures (described in the phase diagram), the system also has a Curie temperature, that changes from zero (paramagnetic) at $x = 0$ up to 920 K (hard magnet) at $x = 5$. However, at $x_c \sim 1.9$ we found a sudden increase of T_C; and this feature could be explained in terms of percolation theory.

Concerning the advantage of the magnetocrystalline anisotropy on the magnetocaloric properties, we found that for $x \lesssim 2.15$ the magnetic entropy change peak related to the spin reorientation merges with that around T_C, leading therefore to quite large full width at half maximum (δT_{FWHM}); for instance, $\delta T_{FWHM} = 160$ K for $x = 2.15$, which represents 8 times higher than the Gd value. Thereby the RCP (relative cooling power) reaches appreciable values which are comparable to the Gd ones.

The study of this group of alloys will proceed with the production of single crystal samples of $PrNi_{5-x}Co_x$, with x=2.7, by the Czochralski method using a radio frequency oven in the University of Campinas. Also, we will continue the study of our samples with Magnetic Circular Dichroism (XMCD) measurements as a function of temperature in the K edge of the Co and the L edge of the Pr (from 12 K to 300 K) so as to study the contribution of each of the magnetic moments (Pr and Co) individually, to see at which temperature and composition the crystal field and hexagonal structural field give rise to the cancelation of the Pr magnetic moment, also to understand why the MCE maximum occurs at x=2.5 and finally to study the coupling of magnetic moments associated with the two magnetic sublattices.

5.3 RNi_2 alloy

Three RNi_2 samples were produced (R=Gd;Nd;Tb). X-Ray diffraction analysis revealed that only the $GdNi_2$ and the $TbNi_2$ samples were single phased, but the $NdNi_2$ sample presented secondary phases, most probably due to an unsuccessful vacuuming of the quartz tubes that gave rise to the presence of oxygen in the samples. This whoever did not disturb our results too much, as the two secondary phases found weren't magnetic and the measurement could be easily normalized by the mass of the desired phase.

5.4 Conferences and Publications

5.4.1 Conferences (participation)

1 - V Jornadas do CICECO
University of Aveiro, Portugal
January, 24-25th, 2008;

2 - 2$^n d$ Workshop on Low-Dimensional Structures: Properties and Aplications (WLDS'2008)
University of Aveiro, Portugal
January, 31 - February, 1, 2008;

3 - 14th Workshop on Magnetism and Intermetallics
University of Coimbra, Portugal
February, 14-15th, 2008;

4 - IEEE International Magnetics Conference
Municipal Conference Center of Madrid, Spain
May, 4-8th, 2008;

5.4.2 Conferences (presentations)

Oral Presentations

1 - **J.V. Leitão**, D.L. Rocco, J.S. Amaral, M.S. Reis, V.S. Amaral, N. Martins and P.B. Tavares
Influence of the magnetic anisotropy on the magnetic entropy change of the Ni_2MnGa memory shape alloy
14^{th} Workshop on Magnetism and Intermetallics
University of Coimbra, Portugal
February, 14-15th, 2008;

2 - D.L. Rocco, J.S. Amaral, **J.V. Leitão**, V.S. Amaral, M.S. Reis, R.P. Fernandes, J.P. Araújo, A.M. Pereira, P.B. Tavares, Nuno V. Martins and A.A. Coelho
Influence of the magnetocrystalline anisotropy on the magnetocaloric properties of $PrNi_{5-x}Co_x$: from spin reorientation to percolation processes
XXXI Encontro Nacional de Física da Matéria Condensada
Convention Cente of the Hotel Majestic, Águas de Lindóia, Brazil
May, 5-9th, 2008;

Poster Presentations

1 - **J.V. Leitão**, D.L. Rocco, J.S. Amaral, M.S. Reis, V.S. Amaral, N. Martins and P.B. Tavares
Influence of the magnetic anisotropy on the magnetic entropy change of the Ni_2MnGa memory shape alloy
V Jornadas do CICECO
University of Aveiro, Portugal
January, 24-25th, 2008;

2 - **J. V. Leitão**, D. L. Rocco, J. S. Amaral, M. S. Reis, V. S. Amaral, R. P. Fernandes, N. V. Martins and P. B. Tavares
Influence of the magnetic anisotropy on the magnetic entropy change of Ni_2MnGa memory shape alloy

IEEE International Magnetics Conference
Municipal Conference Center of Madrid, Spain
May, 4-8^{th}, 2008;

3 - **J. V. Leitão**, D. L. Rocco, J. S. Amaral, M. S. Reis, V. S. Amaral, R. P. Fernandes, N. V. Martins and P. B. Tavares
Influence of the magnetic anisotropy on the magnetic entropy change of Ni_2MnGa memory shape alloy
XXXI Encontro Nacional de Física da Matéria Condensada
Convention Cente of the Hotel Majestic, Águas de Lindóia, Brazil
May, 5-9^{th}, 2008;

5.4.3 Publications

1 - Influence of the magnetic anisotropy on the magnetic entropy change of $Ni_2Mn(Ga,Bi)$ memory shape alloy
J. V. Leitão, D. L. Rocco, J. S. Amaral, M. S. Reis, V. S. Amaral, R. P. Fernandes, N. V. Martins and P. B. Tavares
IEEE Transactions on Magnetics;
(accepted but not yet published)

2 - Influence of the magnetocrystalline anisotropy on the magnetocaloric properties of $PrNi_{5-x}Co_x$: from spin reorientation to percolation processes
D.L. Rocco, J.S. Amaral, **J.V. Leitão**, V.S. Amaral, M.S. Reis, R.P. Fernandes, J.P. Araújo, A.M. Pereira, P.B. Tavares, Nuno V. Martins and A.A. Coelho
Physical Review B
(submitted)

3 - Conventional and anisotropic magnetocaloric effect of RNi2 (R=Nd, Gd, Tb) intermetallic compounds
E. J. R. Plaza, V. S. R. de Sousa, P. J. von Ranke, A. M. Gomes, D. L. Rocco, **J.V. Leitão** and M. S. Reis
(not yet submitted)

Bibliography

[1] Debye P. *Ann. Phys.* **81** (1926) 1154.

[2] Giauque W.F. *J. Am. Chem. Soc* **49** (1927) 1864.

[3] Giauque W.F. and MacDougall D.P. *Phys. Rev.* **43** (1933) 768.

[4] K. A. Gschneidner J. and Pecharsky V.K. *Int. Jour. of Refri.* **pre-publication** (2008) 1.

[5] Jr K.A.G., Pecharsky V.K. and Tsokol A.O. *Rep. Prog. Phys.* **68** (2005) 1479.

[6] Tishin A. and Spichkin Y. *The Magnetocaloric Effect and its Applications* .

[7] Pecharsky V.K. and K. A. Gschneidner J. *Phys. Rev. Lett.* **78** (1997) 4494.

[8] Choe W., Pecharsky V.K., Pecharsky A.O., K. A. Gschneidner J., V. G. Young J. and Miller G.J. *Phys. Rev. Lett.* **84** (2000) 4617.

[9] Pecharsky V.K., Holm A.P., K. A. Gschneidner J. and Rink R. *Phys. Rev. Lett.* **91** (2003) 197204.

[10] Morellon L., Arnold Z., Magen C., Ritter C., Prokhnenko O., Skorokhod Y., Algarabel P.A., Ibarra M.R. and Kamarad J. *Phys. Rev. Lett.* **93** (2004) 137201.

[11] Spichkin Y.I., Pecharsky V.K. and K. A. Gschneidner J. *J. Appl. Phys.* **89** (2001) 1738.

[12] Thuy T. *Proc. 8th Asia-Pacific Physics Conf. (Singapore: World Scientific)* **8** (2001) 354.

[13] Morellon L., Magen C., Algarabel P.A., Ibarra M.R. and Ritter C. *Appl. Phys. Lett.* **79** (2001) 1318.

[14] Ivchenko I. *Adv. Cryog. Eng.* **46** (2000) 405.

[15] Thuy N., Chen Y., Yao Y., Wang C., Lin S., Ho J., Nguyen T., Thang P., Klaasse J., Hien N. and Tai L. *J. Magn. Magn. Mater* **262** (2003) 432.

[16] Hu F.X. *J. Phys: Condens. Matter* **12** (2000) 2691.

[17] Fujita A., Fujieda S., Hasegawa Y. and Fukamichi K. *Phys. Rev. B* **67** (2003) 104416.

[18] Fujita A., Fujieda S., Fukamichi K., Mitamura H. and Goto T. *Phys. Rev. B* **65** (2001) 014410.

[19] Fujieda S., Fujita A. and Fukamichi K. *Proceedings of the First IIR International Conf. on Magnetic Refrigeration at Room Temperature, Montreux-Switzerland* (2005) 193.

[20] Wada H. and Tanabe Y. *Appl. Phys. Lett* **79** (2001) 3302.

[21] Gama S., Coelho A.A., de Campos A., Carvalho A.M.G., Gandra F.C., von Ranke P.J. and de Oliveira N.A. *Appl. Phys. Lett* **93** (2004) 237202.

[22] Tegus O., Brück E., Zhang L., Dagula, Buschow K. and de Boer F. *Physica B* **319** (2002) 174.

[23] Hu F.X., gen Shen B. and rong Sun J. *Appl. Phy. Lett.* **76** (2000) 3460.

[24] Zhou X., Li W., Kunkel H.P. and GwynWilliams. *J. Phys: Condens. Matter* **16** (2004) L39.

[25] Morelli D.T., Mance A.M., Mantese J.V. and Micheli A.L. *J. Appl. Phys.* **79** (1996) 373.

[26] Amaral J.S. and Amaral V.S. *J. Magn. Magn. Mater.* **272** (2004) 2104.

[27] Chen H., Lin C. and Dai D. *J. Magn. Magn. Mater.* **257** (2003) 254.

[28] Reis M.S., Amaral V.S., Araújo J.P., Tavares P.B., Gomes A.M. and Oliveira I.S. *Phys. Rev. B* **71** (2005) 144413.

[29] Chen P., Du Y.W. and Ni G. *Europhys. Lett.* **52** (2000) 589.

[30] Wang D., Liu H., Tang S., Yang S., Huang S. and Du Y. *Phys. Lett. A* **297** (2002) 247.

[31] de Oliveira N.A., von Ranke P.J. and Troper A. *Phys. Rev. B* **69** (2004) 064421.

[32] von Ranke P.J., Nóbrega E.P., de Oliveira I.G., Gomes A.M. and Sarthour R.S. *Phys. Rev. B* **63** (2001) 184406.

[33] Dan'kov S., Ivtchenko V., Tishin A., K.A. Gschneidner J. and Pecharsky V. *Adv. Cryog. Eng.* **46** (2000) 397.

[34] Canepa F., Napoletano M. and Cirafici S. *Intermetallics* **10** (2002) 731.

[35] Niua X., Jr. K.G., Pecharskya A. and Pecharsky V. *J. Mag. Mag. Mater.* **234** (2001) 193.

[36] Ilyn M.I., Tishin A.M., K A Gschneidner J., Pecharsky V.K. and Pecharsky A.O. *Cryocoolers 11 ed R G Ross Jr (New York: Kluwer/Plenum)* (2001) 457.

[37] Pecharsky V.K. and Gschneidner K.A. *Int. Jour. of Refri.* **29** (2006) 1239.

[38] Zhou X., Li W., Kunkel H. and Williams G. *Journ. Phys. Cond. Mat.* **16** (2004) 39.

[39] Khovailo V., Takagi T., Tani J., Levitin R., Cherechukin A., Matsumoto M. and Note R. *Phys. Rev. B* **65** (2002) 92410.

[40] Albertini F., Canepa F., Cirafici S., Franceschi E., Napoletano M., Paoluzi A., Pareti L. and Solzi M. *Jour. Magn. Magn. Mat.* **272-276** (2004) 2111.

[41] Vasil'ev A., Bozhko A., Khovailo V., Dikshtein I., Shavron V., Buchelnikov V., Matsumoto M., Suzuki S., Takagi T. and Tani J. *Phys. Rev. B* **59** (1999) 1113.

[42] Chernenko V.A. and Besseghini S. *Sens. Act. A* (2007).

[43] Brück E. *Jour. Phy. D: Ap. Phy.* **38** (2005) R381.

[44] Stadler S., Khan M., Mitchell J., Ali N., Gomes A.M., Dubenko I., Takeuchi A.Y. and Guimarães A.P. *Ap. Phy. Lett* **88** (2006) 192511.

[45] Nishihara H., Komiyama K., Oguro I., Kanomata T. and Chernenko V. *Jour. All. Comp* **442** (2007) 191.

[46] Leitão J.C.V. *Magnetocaloric effect of Ni2Mn(Ga,Bi) shape memory alloys* (Universidade de Aveiro, Aveiro, 2007) .

[47] Ayuela, Enkovaara J. and Nieminen R.M. *Jour. Phy. Cond. Mat.* **14** (2002) 5325.

[48] Aliev A., Batdalov A., Bosko S., Buchelnikov V., Dikshtein I., Khovailo V., Koledov V., Levitin R., Shavrov V. and Takagi T. *Jour. Magsm. Mag. Mat.* **272-276** (2004) 2040.

[49] Khovailo V., Novosad V., Takagi T., Filippov D., Levitin R. and Vasil'ev A. *Phys. Rev. B* **70** (2004) 174413.

[50] Gomes A.M., Khan M., Stadler S., Ali N., Dubenko I., Takeuchi A.Y. and Guimarães A.P. *Jour. Ap. Phy* **99** (2006) 08Q106.

[51] Söderberg O., Koho T., Sammi T., Liu X., , Sozinov A., Lanska N. and Lindroos V. *Mat. Sci. Eng. A* **378** (2003) 389.

[52] Chen X.Q., Yang F.J. and Qin Z.X. *Phys. Stat. Sol.* **224** (2007) 1047.

[53] Lanska N., Söderberg O., Sozinov A., Ge Y., Ullakko K. and Lindroos V.K. *Jour. App. Phys.* **95** (2004) 8074.

[54] Pons J., Chernenko V.A., Santamarta R. and Cesari E. *Acta Mater* **48** (2000) 3027.

[55] Chernenko V.A. *Scr. Mater.* **40** (1999) 523.

[56] Smith J. *Jour. Phys. F Mat. Phys* **8** (1978) 2139.

[57] Chernenko V.A., Cesari E., Kokorin V.V. and Vitenko I.N. *Scr. Metall. Mater.* **33** (1995) 1239.

[58] Velu E.M.T., Obermyer R.T., Sankar S.G. and Wallace W.E. *IEEE Trans. Magn.* **25** (1989) 3779.

[59] von Ranke P.J., Pecharsky V.K., Gschneidner K.A. and Korte B.J. *Phys. Rev. B* **58** (1998) 14436.

[60] Kubota M., Folle H.R., Buchal C., Mueller R.M. and Pobell F. *Phys. Rev. Lett.* **45** (1980) 1812.

[61] Ermolenko A.S., K. A.V. and Rozhda A.F. *IEEE Trans. Magn.* **13** (1977) 1339.

[62] Chuang Y.C., Wu C.H., Chang S.C. and Li T.C. *J. Less-common. Met.* **97** (1984) 245.

[63] Andreyev A.V., Deryagin A.V. and Zadvorkin S.M. *Phys. Met. Metall.* **60** (1985) 96.

[64] Mal H.H.V., Buschow K.H.J. and Kuijpers F.A. *J. Less-common. Met.* **32** (1973) 289.

[65] Ermolenko A.S. *IEEE Trans. Magn.* **MAG-15** (1979) 1765.

[66] von Ranke P.J., Mota M.A., Grangeia D.F., Gandra A.M.G.C.F.C.G., Coelho A.A., Caldas A., de Oliveira N.A. and Gama S. *Phys. Rev. B* **70** (2004) 134428.

[67] Rocco D., Amaral J., Leitão J., Amaral V., Reis M., Fernandes R., Araújo J., Pereira A., Tavares P., Martins N.V. and Coelho A. .

[68] Chuang Y.C., Wu C.H. and Chang Y.C. *Jour. Less-common. Met.* **84** (1982) 201.

[69] Coroian N., Klosek V., and Isnard O. *J. All. Comp* **427** (2007) 5.

[70] Zlotea C. and Isnard O. *J. All. Comp* **346** (2002) 29.

[71] Stauffer D. and Aharony A. *Introduction to Percolation Theory* .

[72] Ibarra M.R., Morellon L., Algarabel P.A. and Moze O. *Phys. Rev. B* **44** (2007) 073902.

[73] Gschneidner K.A. and Pecharsky V.K. *Annu. Rev. Mater. Sci.* **30** (2000) 387.

[74] Yakinthos J. and Paccard D. *Sol. St. Comm.* **10** (1972) 989.